MASTER

Measuring and modelling the temperature profile during biomass fixed bed combustion, with special attention on the release of species from the fuel bed

van de Geijn, Robert

Award date:
2001

Measuring and modelling the temperature profile during biomass fixed bed combustion, with special attention on the release of species from the fuel bed

Robert van de Geijn
May, 2001

Supervisors: Dr.ir.H.P.v.Kemenade
Dipl.-Ing. A. Weissinger

Eindhoven, University of Technology
Faculty Mechanical Engineering
Section Process Technology

Summary

Investigation of biomass fixed bed combustion is getting more important due to the small scale combustion character, which solves a disadvantage of biomass combustion: high transportation costs due to the low energy content. At Eindhoven University of Technology, research is done on the release of pollutant species (NO_x, CO, etc.) during biomass fixed bed combustion. This research is performed in co-operation with BIOS Bio-energy Systems, Graz (Austria).

A numerical 1-D model is developed to describe the temperature profile in the fuel bed. This model consists of physical laws and kinetics. The model divides the bed into layers, whereby for each layer the energy and mass balance is defined. In this report a global mechanism is used to describe the conversion of biomass into gas, wood and char.

Beside that, experiments are performed to investigate the influence of the airflow, oxygen concentration and temperature on the release of species from the fuel bed. The data obtained during the experiments is also used to check the model concerning the temperature profile and mass decrease.

Experimental data showed a clear relation on the bed temperature of the oxygen concentration and the airflow respectively. In his turn the temperature is related to the release of species from the fuel bed, which makes it possible to implement the release of species indirect in the model, which describes the bed temperature. However, further refinement of the model is necessary to describe the temperature profile in the bed correctly.

Nomenclature

a	pre-exponential factor	$[s^{-1}]$
a_v	specific area	$[m^2/m^3]$
A	area	$[m^2]$
B	transmission	[-]
c_p	specific heat at constant pressure	$[Jkg^{-1}K^{-1}]$
C	concentration	$[kgm^{-3}]$
d	diameter	[m]
D	mass diffusivity	$[m^2s^{-1}]$
E	energy	[J]
E	activation energy	$[Jmole^{-1}]$
E_b	emissive power	$[Wm^{-2}]$
f	shape factor	[-]
F	view factor	[-]
h	heat transfer coefficient	$[Wm^{-2}K^{-1}]$
ΔH	enthalpy	$[Jmole^{-1}]$
J	radiosity	$[Wm^{-2}]$
k	thermal conductivity	$[Wm^{-1}K^{-1}]$
k	reaction constant	$[s^{-1}]$
l	length	[m]
m	mass	[kg]
m	reaction order	[-]
$\dot{m}$	massflow	$[kgs^{-1}]$
M	mass	[kg]
q	heat flux	[W]
R	radius	[m]
R	universal gas constant	$[Jkg^{-1}K^{-1}]$
t	time	[s]
T	temperature	[K]
u	velocity	$[ms^{-1}]$
U	velocity	$[ms^{-1}]$
V	volume	$[m^3]$
V_{spec}	molar volume of an ideal gas	$[m^3mole^{-1}]$
x	length scale	[m]
X	conversion	[-]

Greek letters

α	thermal diffusivity	$[m^2s^{-1}]$
ε	emissivity	[-]
η	conversion rate	[-]
λ	stochiometric factor	[-]

ν	kinematic viscosity ($\nu = \mu/\rho$)	$[m^2s^{-1}]$
ρ	density	$[kgm^{-3}]$
σ	Stefan-Boltzmann constant	$[Wm^{-2}K^{-4}]$
Φ	Thiele modulus	[-]
ψ	air ratio	[-]

Subscripts

$()_B$	biomass	$()_{kin}$	kinetic
$()_c$	convection	$()_p$	particle
$()_C$	char	$()_r$	radiation
$()_{cond}$	conduction	$()_{rad}$	radiation
$()_{conv}$	convection	$()_{vap}$	vaporisation
$()_g$	gas	$()_w$	wood

Dimensionless groups

Bi	Biot number
Nu	Nusselt number
Pe	Peclet number
Pr	Prandtl number
Re	Reynoldsnumber
Sc	Schmidt number
Sh	Sherwood number

Contents

Preface

Investigation in the field of renewable energy sources has always been a field of personal interest. The research performed for my master thesis gave me the opportunity to do research in this particular field. Research is performed at the Eindhoven University of Technology and partly at BIOS Bio-energy Systems, Graz (Austria).

During my master thesis I performed a project consisting of experimental and numerical work. The diversity of my project gave me the opportunity to learn in all kind of fields, from practical experiences during the start-up phase of the measurements to specific modelling experiences. Furthermore, I had the opportunity to develop myself personally, due to the fact that one part of the research is performed abroad. I experienced my stay in Austria as an extra value of my study Mechanical Engineering. Nice experiences and challenges, like having contact with people all over the world, getting in contact with cultural differences, speaking other languages and investigating the totally new surroundings made this period for me an unforgettable time. All in all a year in which I learned a lot on educational level as well as personally.

During my project several people helped me, from which I want to thank some people especially.

First of all I want to thank Alex, who always had time to advice me and to discuss things. You and Thomas turned the measuring days into pleasant days. Furthermore, I want to thank Büro 3 and all the other friends in Graz for the sociability, which made my stay in Graz a pleasant period. I will never forget the barbecue parties, harvesting the grapes and all those other nice experiences we had together!

Of course I want to thank Erik van Kemenade. Thanks for the freedom you gave me during my project, for visiting me in Graz to control my progress and for the nice discussions we had on practical problems during the measurements as well as on the modelling field. Beside Erik, I want to thank Hans Kuerten for helping me with practical modelling advises.

Koen and Marcel, thanks for being four-day-cabdrivers by bringing us to Graz! Michiel thanks for helping me! And of course I want to thank Leeman for the great time we had in Austria.

At the end I want to thank my friends and family for supporting me and for all the pleasure we had during the past years!

Robert van de Geijn
Eindhoven
May 2001

1 Introduction

Renewable energy sources become more important, due to an expected shortage of fossil fuels in the future and due to emerging environmental concern. The main problems caused by the combustion of fossil fuels are the greenhouse effect, acid rain, the remaining ash containing heavy metals and the depletion of the ozone layer. A renewable energy source with a good prospect is biomass. It is a renewable energy source since it is carbon dioxide neutral if a sustainable forest/agricultural management is given. Therefore, it has no extra contribution to the greenhouse effect. It is called neutral due to the fact that the amount generated during combustion is, in turn, equal to the amount used up for growing biomass. However, disadvantages of biomass combustion are the remaining ash, high transportation costs due to the low energy content and the pollutant emissions like NO_x, CO and dust.

The project described in this report is performed within the framework of a R&D project focussing on the release of species from biomass fuel beds during fixed bed combustion, with special attention on nitrogen species. Reducing the nitrogen release is necessary due to the following contributions of nitrogen species on the environment: acid rain, the greenhouse effect and the depletion of the ozone layer. In [Geijn, 2000] more details concerning the influence of nitrogen species on the environment are outlined.

The purpose of the research described in this report is to develop a model to predict the release of species from the fuel bed, which can be used as input data for the modelling of gas phase combustion above the fuel bed. Modelling of the gas phase combustion is necessary to design a furnace better concerning the efficiency and emissions. At the moment the design of the furnace is a trial and error process. Therefore, it is necessary to describe the species release from the fuel bed more accurately in order to gain correct input data for the gas phase combustion modelling. The investigation to the release of species, with special attention for the nitrogen species is performed by A. Weissinger, making his PhD-project on this subject.

In order to know which parameters influence the release of nitrogen species, it is necessary to perform experiments. By performing these experiments it is possible to find trends concerning the nitrogen release. Developing test runs to investigate influence parameters, like temperature, air flow and oxygen concentration and performing the experiments is one part of the research described in this report. Beside this, a first set-up is made to model the release of species with physical laws and chemical kinetics. So, the purpose of the research presented in this report is to find the influence of certain parameters on the release of nitrogen species from a grate furnace and to develop a model, which is capable to describe the temperature development and ignition front in the fuel bed. Furthermore, a first approach will be made to model the release of species from the fuel bed.

Investigation on a grate furnace is performed by BIOS Bio-energy systems. However, problems occurred during the experiments, because the boundary conditions of the gas phase

above the fuel bed are difficult to determine. Beside that the in-situ FT-IR measurement method is more accurate for measurements above a pot furnace, because the path length and temperature gradient is smaller. Therefore, a comparison between a grate furnace and the pot furnace used during experiments is made in chapter 2, in which is explained at which conditions it is possible to simulate a grate furnace with a pot furnace.

In chapter 3 a 1D-model is discussed. The model consists of physical laws describing the temperature in the bed and the vaporisation of the water content. Beside that, the model consists of kinetic laws describing the temperature and the release of species during reaction. The chemical reactions are approximated by a global mechanism consisting of the conversion of wood into gas, tar and char.

In the next chapter 4 the experimental set-up is described. Starting with the purposes of the measurements, which are based on the results of a literature research, already performed and described in [Geijn, 2000]. After the purposes of the experiments are discussed, the measurement equipment used is presented, followed by the fuel type used and the required data treatment.

The results of the measurements are presented in chapter 5. This chapter starts with the explanation of the temperature profile in the bed. After that, a relation is deduced between the temperature profile and the species released. The chapter ends with the description of the influence of the parameters investigated on the release of species from the biomass fuel bed.

In the chapter 6 the results from the model are compared to the data of the measurements. The validity of the model will be discussed and suggestions will be made for optimisation of the model.

Conclusions concerning the research made will be presented in the concluding chapter 7. Beside this, recommendations are made for further research in this topic.

2 Grate furnace compared to a pot furnace

Biomass fuels have a low heating value compared to fossil fuels. Consequently biomass combustion is especially suitable for small-scale energy production close to the source material. Small scale biomass combustion plants, up to $10MW_{th}$ [Geijn, 2000], normally rely on fixed bed or grate furnaces. However, these plants are not as well investigated as the larger scale fluidized bed plants, for which the conversion process is better controllable. In a fluidized bed is the contact between solid and gas better, is the temperature more uniform and is the heat transfer in the bed better compared to grate and fixed bed combustion. Because of these differences, the results obtained during fluidized bed conditions are different and the conversion of biomass during grate and fixed bed combustion has to be investigated. In this report investigation is done for a grate furnace for which an example is given in figure 2.1.

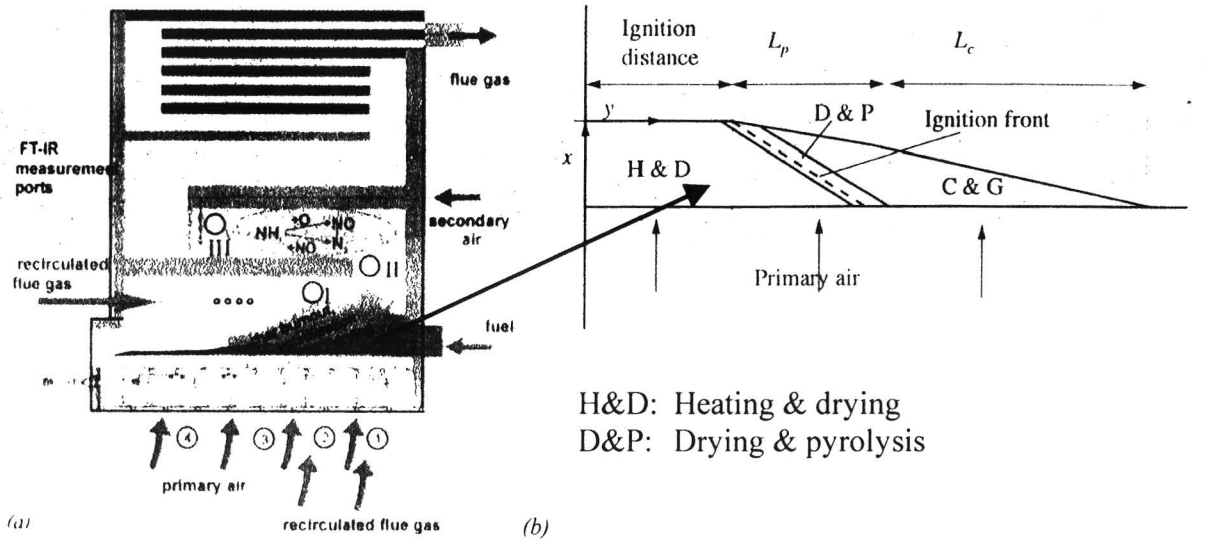

figure 2.1: ***(a) Schematic overview of the travelling grate furnace [Weissinger] (b) visualisation of the fuel bed with the different zones during grate combustion [Saastamoinen, 1999]***

The fuel entering the hot furnace is heated by the hot gasses and by the radiation from the heating elements in the furnace. Ignition starts at the top of the fuel bed and propagates downwards through the bed, whereby the fuel travels horizontal with a velocity, U as illustrated in figure 2.2.

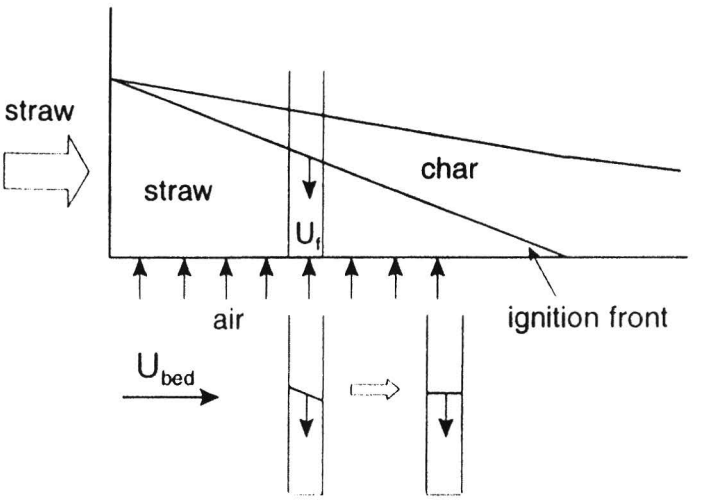

figure 2.2: ***Visualisation of the horizontal velocity, U_{bed} and vertical velocity, U_f occurring in a fuel bed during grate combustion [Lans]***

At steady state the fuel is supposed to be transported continuously over the grate with a velocity, U_{bed}. The ignition front propagates downwards with a velocity, U_f (figure 2.2). By calculating the Peclet number it is possible to find the relevance importance of the horizontal gradient compared to the vertical gradient [Lans, 1998]. The Peclet number is defined as follows:

$$Pe = \frac{U_{bed} \cdot l_{bed}}{\alpha} = \frac{U_{bed} \cdot l_{bed}}{\left(k / \rho \cdot c_p \right)} \qquad (2\text{-}1)$$

Where U is the velocity, l is the length and α is the diffusion coefficient. With a bed velocity, U of 1.5e-3 ms^{-1}, a length of 3 m and a diffusion coefficient of 1.7e-7 m^2s^{-1} the Peclet number is in the order of 10^5 for heat transport in the horizontal direction. The diffusion coefficient is based on a thermal conductivity, k of 0.1 $Wm^{-1}K^{-1}$, a density of the bed, ρ of 250 kgm^{-3} and a specific heat, c_p of 2.3e3 $Jkg^{-1}K^{-1}$. This high value of the Peclet number means that it is possible to follow a package of biomass fuel in the grate furnace over the time. Therefore, it is possible to simulate the grate combustion with a pot furnace, whereby the propagation front moves only vertical as shown in the figure above.

The modelling and experiments are performed with a pot furnace in order to simulate a grate furnace. This simplification is based on derivation described above.

3 Model of the combustion process

In order to predict the release of species from a fuel bed, a model is developed. The model consists of two parts: the physical model, describing the temperature development in the bed and the kinetic model, describing the reactions in the bed. The way of modelling the temperature distribution in the fuel bed is outlined in the following paragraph 3.1. In this paragraph the heating up of the bed is described followed by the evaporation of the water. In paragraph 3.3 the kinetic model is discussed, followed by a brief summary of the model.

3.1 Modelling of the temperature

During the heating and combustion of the fuel bed, several heat fluxes have an influence on the temperature distribution in the bed. In figure 3-1 the different heat fluxes in the furnace are shown.

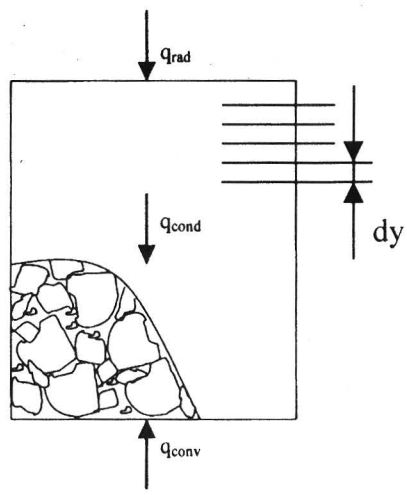

figure 3-1: Heat fluxes through the furnace

In the figure above two heat fluxes are visualised. A heat flux caused by an airflow from under the bed and a heat flux caused by radiation from above the fuel bed. The radiation above the fuel bed causes a conductive heat flux through the fuel bed. During the calculation the bed is divided in layers, which is explained in more detail in appendix A.2, the discretization process. This means that the heat balance for the upper layer of the fuel bed is different from the heat balance in the bed. The heat balances are discussed in the next paragraph.

Heat balance in the bed:
The conductive heat flux through the bed, which is caused by the radiation from above the bed, is defined as follows:

$$q'' = k_{eff} \cdot \frac{\partial T}{\partial x} \qquad (3\text{-}1)$$

With k defined as the effective thermal conductivity through the fuel bed, which depends of the radiation between the particles in the fuel bed. This dependency will be explained in more detail in paragraph 0. The heat flux caused by the mass flow from under the fuel bed can be modelled as forced convection. This heat flux is defined as follows:

$$q_c'' = h \cdot \Delta T \qquad (3\text{-}2)$$

Where h is the heat transfer coefficient, which will be defined in more detail in paragraph 3.1.2. These two heat fluxes are equal to the internal energy change of a control volume.

$$q = \frac{dE}{dt} \qquad (3\text{-}3)$$

The internal energy change of an incompressible substance is proportional to the change in temperature. Rewriting equation 3-3 gives the following relation for the internal energy of a control volume in the fuel bed:

$$q = \frac{dE}{dt} = \rho \cdot c_p \cdot V \cdot \frac{dT}{dt} \qquad (3\text{-}4)$$

This change in internal energy is equal to the net heat transfer caused by the airflow and conductivity. Substituting equation 3-1 and equation3-2 together into equation 3-4 yields

$$\rho \cdot c_p \cdot V \cdot \frac{\partial T}{\partial t} = k \cdot A \cdot \frac{\partial T}{\partial x} + S \qquad (3\text{-}5)$$
$$with: S = q_c + q_{vap} + q_{kin}$$

The second term on the right side of equation 3-5 is a source term. This term represents the energy released during the conversion of biomass fuel, q_{kin} and the energy required for drying the biomass fuel, q_{vap}. With the above-mentioned equation it is possible to describe the temperature development in time of a control volume in the bed.

Heat balance in the upper layer:
The upper layer of the fuel bed will be heated directly from the radiation elements. The heat fluxes for the upper layer are visualised in the figure above.

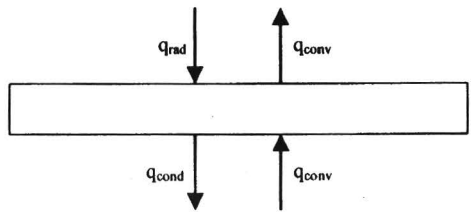

figure 3-2 ***heat fluxes in the upper layer***

The heat balance for the upper layer is defined in the equation below.

$$\rho \cdot c_p \cdot V \cdot \frac{\partial T}{\partial t} = q_{cond} + S \qquad (3\text{-}6)$$
$$with: S = q_c + q_r + q_{vap} + q_{km}$$

The conductive heat flux leaving the upper part and the convective heat flux through the layer are described on the same way as in the other layers of the fuel bed. A radiation heat flux, q_r is caused by the sidewall and upper wall of the furnace. The temperature of the wall is measured and set at a certain temperature during the measurements. It is assumed that the temperature of the wall is constant in time, isothermal and uniform over the area. The temperature of the sidewall is set at 450°C and the upper wall is set at 750°C during the measurements in order to heat the fuel till ignition temperature. Because of these areas with a different temperature, the heat flux by radiation is calculated by the matrix inversion method, which is outlined in appendix A.1 [Kreith, 1986].

In order to solve the heat balances described above numerically it is necessary to discretizate the equations. The method used is the finite-difference method. This method divides the fuel bed in control volumes, which are not overlapping each other. It is assumed that the temperature distribution can be modelled one dimensional, because the horizontal gradient is negligible during grate combustion as discussed in chapter 2. This is not in accordance with the measurements made, which showed a horizontal temperature gradient in the pot furnace. However, for simplicity and because of the symmetry of the pot furnace a one-dimensional model is used to describe the temperature profile in the bed. The discretization process is discussed in appendix A.2 for the heat balance of a layer in the fuel bed. After discretization the following equation yields for the energy equation.

$$a_P T_P = a_N T_N + a_S T_S + b$$
$$a_P = a_P^0 + a_N + a_S$$
$$a_N = \frac{k_n}{\Delta y}$$
$$a_S = \frac{k_s}{\Delta y} \qquad (3\text{-}7)$$
$$b = a_P^0 T_P^0 + S\Delta y$$
$$a_P^0 = \frac{\rho \cdot c_p \cdot \Delta y}{\Delta t}$$

The most important modelling assumptions are:
- The process is assumed adiabatic. Heat loses to the side are neglected.
- Change in the total mass flow is neglected. The large fraction of inert species in the combustion air often allows this assumption [Gort, 1995].
- A uniform temperature over the layer is assumed. Temperature and concentration gradients in the interior of the particles are neglected.
- Conduction of heat is described with an effective thermal conductivity
- The process is assumed isobaric.

3.1.1 Thermal conductivity

As mentioned before the upper layer of the fuel bed will be heated up by radiation, which causes a conductive heat flux through the fuel bed. Because the biomass is a porous medium, the heat transfer occurs partly by radiation in the pores. This effect can be modelled as an additional term to the thermal conductivity coefficient [Di Blasi, 1993].

$$k_{eff} = \eta \cdot k_B + (1-\eta) \cdot k_C + \psi \cdot k_g + \frac{\sigma \cdot T^3 \cdot d}{\varepsilon} \qquad (3\text{-}8)$$

Where k_B, is the initial value for the thermal conductivity of the biomass, k_C, is the final value for the thermal conductivity of the char residue, k_g, is the thermal conductivity of the gas phase, ψ, is the porosity defined in equation 3-16 and η is the conversion rate. In the equation above, the properties of the layer, during pyrolysis are assumed to be linear dependent of the conversion rate, η, which is defined as follows:

$$\eta = \frac{M_B}{M_B + M_C} \qquad (3\text{-}9)$$

The additional term for radiation, last term on the right side of equation 3-8, is assumed to be achieved by the radiation in spherical pores with a diameter d. Whereby, ε is the emissivity of the fuel and σ is the Stefan Boltzman constant. A similar additional term is described in [VDI, Ka] and is defined as follows:

$$k = \frac{2B + \varepsilon(1-B)}{2(1-B) - \varepsilon(1-B)} \cdot \sigma \cdot 4 \cdot T^3 \cdot d_p \qquad (3\text{-}10)$$

Where B is the transmission, which is determined to be 0.05 based on an emissivity, ε of wood of 0.9 [VDI, Ka7]. An advantage of the definition, described in equation 3-10, is that it is based on the particle diameter, d_p in stead of the pore diameter, d. It is chosen to calculate the effective thermal conductivity with equation 3-8, due to the diversity in particle size of the fuel used. The pore diameter is assumed to be in the range of 10^{-6}m based on [DiBlasi, 1993] and [Beuken, 2000].

3.1.2 Heat transfer coefficient

The heat transfer between a particle and an airflow through the bed material is defined in equation 3-11 [VDI, Gh1].

$$q' = h \cdot \Delta T = h \cdot (T - T_g) \qquad (3\text{-}11)$$

Where T is the temperature in the layer, T_g is the temperature of the flow, and h is the heat transfer coefficient, which is dependent of a flow going through a porous medium. The heat transfer coefficient of a particle can be counted out by making use of the Nusselt number for a single spherical particle, with a stream around it, multiplied by a shape factor.

$$Nu = f_a \cdot Nu_{ssp} \qquad (3\text{-}12)$$

For which the Nusselt number of a single spherical particle, Nu_{ssp} is defined in equation 3-13.

$$Nu_{ssp} = 2 + \sqrt{Nu_{lam}^2 + Nu_{turb}^2}$$

$$with: \quad Nu_{lam} = 0.664 \cdot \sqrt{\mathrm{Re}_\psi} \sqrt[3]{\mathrm{Pr}} \qquad (3\text{-}13)$$

$$Nu_{turb} = \frac{0.037 \cdot \mathrm{Re}_\psi^{0.8} \cdot \mathrm{Pr}}{1 + 2.443 \cdot \mathrm{Re}_\psi^{-0.1} \cdot \left(\mathrm{Pr}^{2/3} - 1\right)}$$

The dimensional numbers described in the equation above are defined below.

$$Nu = \frac{h \cdot d_k}{k}$$

$$\mathrm{Re}_\psi = \frac{\rho \cdot u \cdot d_k}{\mu \cdot \psi} \qquad (3\text{-}14)$$

$$\mathrm{Pr} = \frac{\upsilon}{\alpha}$$

Beside the material properties, like the density, ρ viscosity, v and the diffusivity, α some geometrical parameters are needed to calculate the dimensional numbers. Those parameters are discussed below.

For a fuel bed mainly consisting of spherical particles with the same size the diameter d_k is equal to the diameter of the particle. If the volume specific surface is know it is possible to calculate the diameter, d_k by making use of equation 3-15.

$$d_k = \sqrt{\frac{A_p}{\pi}} \qquad (3\text{-}15)$$

The geometrical surface, A_p from a single particle can be determined with the volume specific surface of the fuel bed and the volume specific number of particles itself.

The velocity, u is the velocity of the flow through an empty cross-section, which has to be corrected by the air ratio due to the smaller cross section in real. The air ratio, the space that is filled with air in the fuel bed, is defined in the equation below.

$$\psi = \frac{V - V_f}{V} \qquad (3\text{-}16)$$

Where V is the volume of the entire fuel bed and V_f is the volume of all the particles together. This volume can be counted out by measuring the mass and divide it by the density of the material.

The shape factors for the different shapes are shown in table 3-1.

table 3-1: The shape factors of different shapes and the validity range [VDI, Gh1]

Shape	*Shape factor f_a*	*Validity range*
Spherical of the same size	$1+1.5(1-\psi)$	$10^{-1} < Re_\psi < 10^4$ Pr, Sc = 0.6-10000
Cylindrical in the range of 0.24<l/d<1.2	1.6	$10^2 < Re_\psi < 10^4$ Pr, Sc = 0.6-1300
Dice	1.6	$10^2 < Re_\psi < 10^4$ Pr, Sc = 0.7

A shape factor of 1.6 is assumed due to the fact that the shape of the bigger particles is similar to dices. The validity range of equation 3-12 is given in the table above, which is in the range measured.

The method above, used to calculate the heat transfer coefficient, assumes particles of the same size with a mean size of air spaces. However, at small Péclet numbers, lower than 1000, the nonuniform distribution of the void fraction leads to big differences in the velocity, and therefore in the Nusselt number. This nonuniform distribution can lead to channel formation at which the superficial velocity is higher than at a section with a lower void fraction [Martin, 1977]. Estimation of channel formation is done by measuring the pressure drop over the bed with and without fuel. The pressure drop with and without fuel is in the same order of size over the range of airflow's measured. This means that the porous plate at the bottom of the bed divides the airflow sufficiently enough and that there is no channel formation occurring, on condition that the bed height is not too big. Therefore, the method described above is valid to calculate the heat transfer coefficient.

3.2 Evaporation of the water

The evaporation of the water content in the fuel is modelled in first approximation by assuming that the evaporation starts at a fixed temperature of 373K. During evaporation the temperature in the layer stays constant. Therefore, the energy storage in time is zero and the energy equation, equation 3-5, transfers into the relation described below.

$$\rho \cdot c_p \cdot V \cdot \frac{\partial T}{\partial t} = 0 \Rightarrow k \cdot A \cdot \frac{\partial T}{\partial \bar{x}} + S = 0 \qquad (3\text{-}17)$$

During evaporation of the water content, the water is converted to vapour. The conversion of water to vapour is an endothermic process. The enthalpy necessary to evaporate the water is modelled in the source term, S described in equation 3-17. The enthalpy required for the evaporation of water is defined in equation 3-18 [Scott Fogler, 1999].

$$H(T) = \int_{T_{R=25°C}}^{T_{va}} c_{p,1} dT + \Delta H_{va}(T_{va}) + \int_{T_{va}}^{T=373K} c_{p,2} dT \qquad (3\text{-}18)$$

Where ΔH_{va} is the change in enthalpy of vaporisation at 25 °C, which is 44.01e3 J/mole according to [Perry, 1997]. The heating up till the vaporisation temperature, T_{va}=25°C, is described by the first term at the right side of the equation above, whereby the specific heat of water is taken at a temperature of 25°C and a pressure of 1 bar. The last term at the right side describes the heating up till the assumed evaporation temperature of 373 K. The specific heat, $c_{p,2}$ is dependent of the temperature and yields the following equation [Perry, 1997].

$$c_{p,2} = 8.22 + 0.00015 \cdot T + 0.00000134 \cdot T^2 \quad [cal/(deg \cdot mol)] \qquad (3\text{-}19)$$

This equation is valid for water vapour in a temperature range of 300-2500 K with an unknown uncertainty. The energy consumed during the evaporation is equal to the product of the mass change in time and the enthalpy as shown in the relation below.

$$q_{va} = \frac{dm}{dt} \cdot H(T) \qquad (3\text{-}20)$$

This heat flux used for the source term in the energy equation, equation 3-17. By rewriting the energy equation and discretizate the equation as discussed in appendix A.2, the following relation yields for the mass change in time for the layers in the bed.

$$\frac{dm}{dt} = \frac{m(t+\Delta t) - m(t)}{\Delta t} = \frac{\left(m_{f,layer} / \rho \right) \cdot \left[a_n \cdot (T_P - T_N) + a_s \cdot (T_P - T_S) - q_c \right]}{H(T) \cdot \Delta y} \qquad (3\text{-}21)$$

At the moment all the initial water is vaporised, the relation described in paragraph 3.1 models the temperature profile again.

By modelling the evaporation as described above, it is assumed that all the water will evaporate out of the particle before ignition. However, this is not totally correct. Depending on the fuel type and particle size a temperature gradient is formed within the fuel. For big particles the temperature of the outer shell is rising above the temperature in the centre of the particle. Therefore, it is possible that the inner side of the particle is still wet as the particle is already ignited [Wartha, 1998]. A correction factor can be determined by measuring the influence of the moisture content on the ignition propagation speed. According to [Saastamoinen 1999b] a linear approximation can be determined between the moisture content and the ignition propagation speed. This correction factor is not determined during this project due to the fact that chipboard is a very dry wood kind, with a constant moisture content.

3.3 Kinetic Model

In literature a lot of kinetic investigation is done, especially in the field of char combustion. In this report kinetic parameters are used, which are found in literature for wood pyrolysis into gas, tar and char. This data is determined by [Thurner, 1981] and is also used by other investigators DiBlasi, 1993], [Beuken, 2000]. As the kinetic data are not determined for the chipboard used during the experiments, it is chosen to perform measurements in the reaction-defined region. This in order to be able to estimate the inaccuracy due to the used kinetic parameters. Estimation of the reaction limitation criteria is described in the next paragraph followed by the kinetics used in paragraph 3.3.2.

3.3.1 Limitation criterion

The conversion process is limited by two different limitation criteria. These are the diffusion and the reaction limitation. During the combustion process it is important to measure in the reaction-limited region. This is necessary in order to be capable to obtain reaction rate data from the measurements. These two limitation regions are illustrated in figure *3-3*.

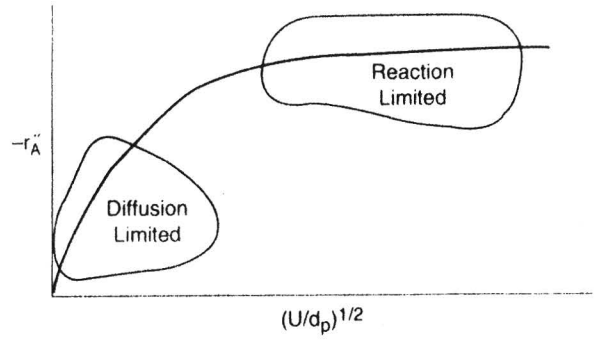

figure 3-3 ***Regions of mass transfer-limited and reaction-limited reactions [Scott Fogler1999]***

With the help of the Sherwood number and the Thiele modulus it is possible to estimate the limitation criterion for an airflow [Kemenade, 1999]. Whereby the Sherwood number corresponds with the Nusselt number for mass transfer. The Sherwood number is calculated for an airflow through a porous medium on a similar way as defined in paragraph 3.1.2 in which the heat transfer coefficient is defined. During this calculation the Prandtl number is

replaced with the Schmidt number [Bejan, 1993]. A definition of the Sherwood number is given in equation 3-22.

$$Sh = \frac{h_m \cdot x}{D} \qquad (3\text{-}22)$$

Where h_m is the mass transfer coefficient and D is the diffusivity. The Sherwood number can be viewed as a 'dimensionless mass transfer coefficient' [Bejan, 1993]. The order of magnitude divides it into two regions. The reaction is not limited by the mass transfer rate for a Sherwood number much higher than one, because the mass transfer rate is much larger compared to the diffusion rate (Sh >> 1). Therefore, the reaction can only be limited by a shortage of reactants. This dependency is defined with the Thiele modulus, which is described in the equation below.

$$\Phi = 0.5 \cdot d_p \cdot \sqrt{\frac{\lambda \cdot k_s \cdot a_v \cdot C_{A,\infty}^{m-1}}{D_{e,0}}} = \frac{reaction\,rate}{diffusion\,rate} \qquad (3\text{-}23)$$

With d_p as the particle diameter, λ as the stochiometric factor of the reaction, k_s as the reaction rate constant, a_v as the specific area per volume, $C_{A,\infty}$ as the concentration of the gas, m as the reaction order and D as the effective diffusion coefficient. Determination of the reaction order and the stochiometric factor is defined in chapter 4.3. The diffusion coefficient is taken as a function of the temperature.

This implies that the conversion is reaction controlled in the case that the Sherwood number, *Sh* is much larger than the Thiele modulus, *Th*. After calculation of this criterion it is found that the Sherwood number is 4.4 times the Thiele modulus at an airflow of 40 l/min. This airflow is taken as the maximum due to the particle transport out of the fuel bed at higher airflows.

Due to this relatively small difference care has to be taken when using the conversion data obtained from the measurements. Beside this disadvantage the release of tar was not measured, which is necessary to determine the kinetics of the global mechanism used. This mechanism is presented in the next paragraph. Another problem is that the combustion conditions in the bed are not constant over the bed. Therefore, kinetic parameters cannot be determined from the measurements described in chapter 4. Comparing the weight loss during conversion between the measurements and the model, can be used to make an estimation of the accuracy of the kinetic.

3.3.2 Kinetics

The chemistry of biomass pyrolysis is a complex system, due to the wide variety of pyrolysis products [Thurner, 1981]. By lumping these products into three groups: gas, tar, and char a mechanism arises consisting of primary and secondary reactions. This mechanism is illustrated in figure 3-4.

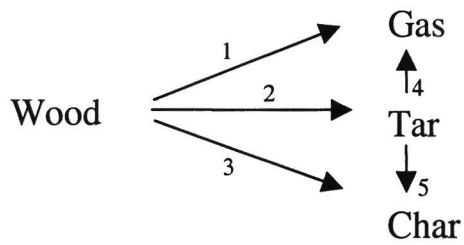

figure 3-4: mechanism of wood pyrolysis [Thurner, 1981]

The decomposition of wood is described by three parallel reactions, called the primary reactions. These reactions are shown in figure 3-4 by reaction number 1, 2 and 3. Whereas the secondary reactions refer to the tar decomposition according to the parallel reactions 4 and 5.

The secondary reactions are neglected during modelling due to opposite direction of the ignition front and airflow. Because of this type of gasifier the tar and gas leave the fuel bed immediately after reaction. Therefore, the decomposition of tar to char and gas is neglected, which also simplified the model.

In equation 3-24 all the reactions, which are used to describe the wood pyrolysis, are defined.

$$\begin{aligned} WOOD &\xrightarrow{k_1} GAS \\ WOOD &\xrightarrow{k_2} TAR \\ WOOD &\xrightarrow{k_3} CHAR \end{aligned} \qquad (3\text{-}24)$$

These reactions are assumed to be first-order and have an Arrhenius type of temperature dependency. The disappearance rate of wood is then defined as follows:

$$\frac{dm_w(t)}{dt} = -(k_1 + k_2 + k_3)\cdot m_w(t) \qquad (3\text{-}25)$$

Whereby the reaction constant, k is defined in equation 3-26.

$$k = a \cdot \exp\left(-\frac{E}{R \cdot T}\right) \qquad (3\text{-}26)$$

With a as the pre-exponential factor, E as the activation energy, R as the universal gas constant and T as the temperature. The activation energy is determined by [Thurner, 1981] for wood pyrolysis at temperatures between 300 and 400°C. However, in practice, pyrolysis will occur at higher temperatures at which the overall pyrolysis rate may also depend on the wood transport properties as discussed above. The exact role and magnitude of these parameters are not investigated by [Thurner, 1981]. Despite of this inaccuracy the kinetics obtained by [Thurner, 1981] are used. In Table 3-2 are the kinetics presented.

Table 3-2: kinetics determined for the global mechanism described in equation 3-24

Reaction	*Pre-exponential factor, a in [s^{-1}] [DiBlasi, 1993]*	*Activation energy, E in [kJ/mole] [Thurner, 1981]*
1	5.16e6	88.6
2	1.48e10	112.7
3	2.66e10	106.5

During reaction the mass concentration decreases according to equation 3-25. Discretization of this equation is done implicit, due to the high kinetic values. This results in the following equation for the mass concentration in time.

$$C_w(t+\Delta t) = \frac{C_w(t)}{1+(k_1+k_2+k_3)\cdot\Delta t} \qquad (3\text{-}27)$$

3.4 Summary

A numerical model is developed in order to describe the temperature profile in a fixed bed. The model divides the bed in layers, whereby over each layer the energy and mass balance is formed. Uncertainties caused by the diversity of the fuel are taken into account, e.g. the porosity. However, some uncertainties caused by the diversity of the fuel had to be approximated. Like the vaporisation of the water content, which will be influenced by the particle diameter. A kinetic model describing the occurring reactions in the bed extends the model. The kinetic model is based on a simplified conversion process consisting of the conversion of wood into gas, tar and char.

After discretization of the equations, describing the heating and combustion process in the bed, a program is written to calculate the temperature profile in time over the bed. Beside that the mass decrease is calculated. This model is written in Matlab©. The program is given in appendix A.3.

4 Experimental

In this chapter an overview is given of the measurements made. First of all the purpose of the experiments is outlined, followed by a short explanation of the measurement. After discussion of the influences measured on the release of species, the measurement equipment used is presented in paragraph 4.2. Special attention is given to the in-situ FT-IR measurement equipment. In the subsequent paragraph the fuel used is discussed, followed by the data evaluation in paragraph 4.4.

4.1 Purpose of the experiments

During the experiments several influence parameters on the release of species are investigated. In this paragraph the purpose of the measurements is discussed in more detail. The exact experimental program and the settings of all the measurements performed are given in appendix B.1.

The first parameter of interest is the airflow rate. A change in airflow rate leads to changes in combustion time and to bed temperature [Geijn, 2000]. Concerning the influence on the release of species there is no uniform trend described in literature. Therefore, the influence of the airflow on the release of species is measured during this investigation. The measuring range is restricted by a minimum airflow at which the reaction front propagates and by a maximum airflow for which the bed is not fluidizing.

For a second parameter, the oxygen concentration in the inlet gas stream, the influence on the nitrogen release is not known. Due to the fact that it is not possible to investigate this influence separately from the gas phase, the general effect has been found. According to literature [Skreiberg, 1997], [Warta, 1998] the effect of an increasing inlet oxygen concentration during gasification leads to a higher conversion of fuel to NO_x. The explanation for this effect can be found in the influence of NH_i, which role changes for different conditions in the gas phase. Under oxidising conditions is the conversion of NH_i to NO dominant and under reduced conditions dominates the conversion of NH_i to N_2 [Geijn, 2000]. Similar effects could appear in the gas present in the fuel bed. That's why, the role of NH_i on the production of NO has been investigated and an optimum in the release of nitrogen species is found.

The mutual effect of both parameters, oxygen concentration and airflow rate, is investigated to find their optimum in nitrogen release compared to CO and to find their joint tendency. The relative importance compared to each other is found in this way.

The measurements are also used to describe the temperature development in the bed as function of the time. This in order to evaluate the model.

4.2 Test facilities

The experiments are performed in a cylindrical fixed-bed reactor, 3500 mm in height and 120 mm in diameter. The fuel is put in a cylindrical holder, 100 mm in height and 95 mm in inner diameter. Both parts are made of carbon fibre strengthened SiC® to avoid reactions of CO, NO, etc. with the wall and to make the wall impermeable to reactor gas. The fuel bed is put into the upper part as shown in figure 4.1 with the dotted lines. Air is introduced through a porous plate at the bottom of the fuel bed. The pot furnace is illustrated in figure 4.1.

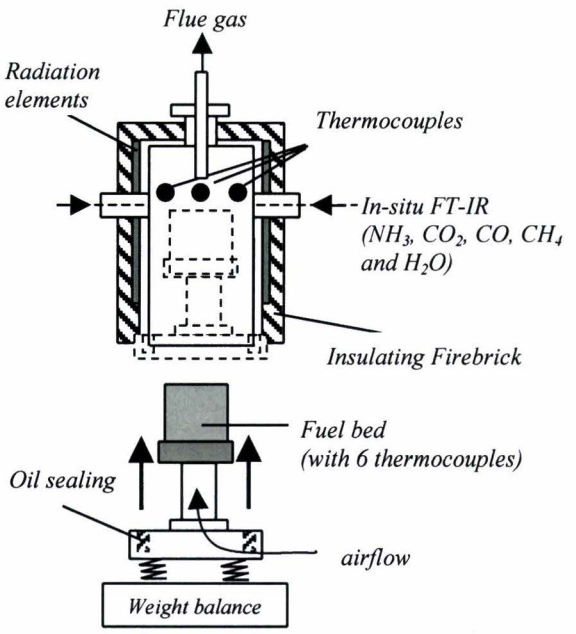

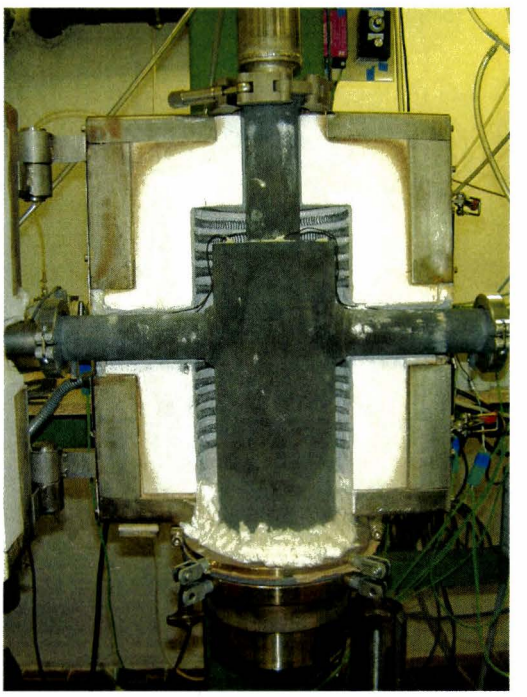

figure 4.1: **Laboratory reactor**

The fuel bed is placed on a weight balance to measure the weight of the fuel bed during reaction. The reactor is built with a thick wall of insulating firebrick. In this insulation layer, radiative heaters heat the reactor, which in his turn heats the fuel. These heating elements are placed at the top and at the upper side of the reactor as shown in figure 4.1. Six thermocouples are placed in the fuel bed in order to measure temperature gradients occurring in the bed. The thermocouples are led into the fuel bed from the bottom through the porous plate. The gas is led out at the top of the reactor.

The whole measurement system, reactor and measurement equipment is shown in figure 4.2.

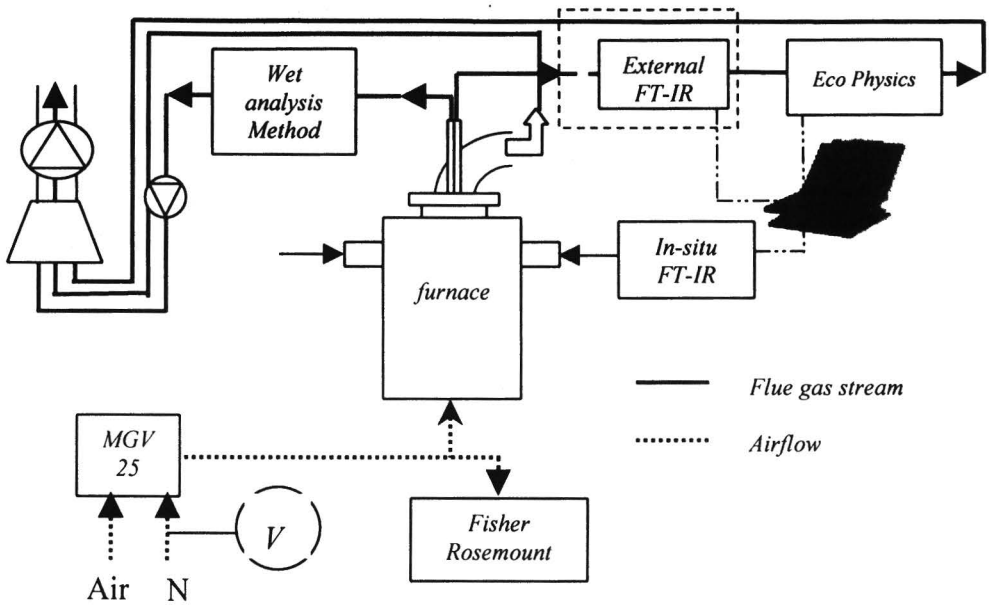

figure 4.2: ***the measuring system***

The flue gas is exhausted by combined influence of a ventilator at the end and the gas analysers. This creates an under pressure in the reactor. The measurement equipment used to measure temperature, pressure, airflow and concentration of species in the flue gas is listed in the next paragraph.

4.2.1 Measurement equipment

In table 4-1 the used measurement equipment for the measured parameters is listed. The placement of the equipment is shown in figure 4.2 and a brief explanation of their use is given in the table below.

table 4-1: Analysers used during the experiments

Parameter measured	*Kind of analyser*	*Used*	*Range*
Temperature	*Thermocouple Type K (NiCrNi) R.S. Components*	*In the fuel bed*	*0 - 1100 K*
Gas flow	*MGV-25 O_2/N_2 0-100% LN Industries*	*Mixing the incoming air flow to get a known concentration of oxygen*	*0 - 100 % O_2*
			< 20 cc/min – 18.2 l/min
	RS Components AWM 5104	*Measuring the nitrogen flow entering the mixing component MGV-25*	*0 - 20 slm*
	Gas sample catheter SP2000 M & C products	*Filtering the flue gas before entering the gas analysers*	-
Diluter	*Dekati Diluter*	*Rarefying the flue gas*	*Dilution rate 1 to 10*
Mass	*Sartarius Gold GP 4102*	*Measuring the mass of the fuel bed*	*0 – 4100 ± 0.01 g*

The gas analysers used during the experiments are listed in the table below. For each equipment the species measured are listed as well as the range. The amount of flue gas extracted is 4 l/min and is diluted 1 to 10 with nitrogen to get the concentration of CO at a save level with regard to explosion danger of the other measuring equipment. Beside that, the flue gas is diluted in order to stop further reactions in the gas phase and to avoid condensation of water.

table 4-2: gas analysers used during experiments

Analyser	*Gasses measured*	*Function*	*Range*
Eco Physics CLD 700 EL hat	*NO, NO_2 and NO_x*		*0 –100 ppm*
Fisher- Rosemount MLT- ½-19''- Analyser	*O_2*	*Checking the oxygen concentration of the inlet airflow*	*0 –22 %*

The performance of the gas analysers and gas flow meters is summarised in appendix B.2. Calibration of the gas analysers is performed at every start-up of the measurement systems.

The concentration of ammonia (NH_3) and hydrogen cyanide (HCN) is determined with the wet analyse method [Keller, 1994], [Zhou, 1998]. In this method the flue gas is led through a solution of NaOH to bind HCN and H_2SO_4 to bind NH_3. The concentration is determined photometric, whereby the colour intensity of the solution is a measure for the concentration. The change in colour intensity occurs after reaction with a reagent. The reagents used in this case are phenol and pyridine-barbituric acid respectively for NH_3 and HCN. During the experiments three bottles were in a row, with two analysers for ammonia followed by an analyser for hydrogen cyanide at the end. The disadvantage of the wet analysis method is that it results in a mean value for HCN and NH_3 over the test run.

Beside the gas analysers listed above, the gas concentrations are also measured in the flue gas directly above the fuel bed. This is done with the in-situ FT-IR absorption spectroscopy . This technique will be discussed in more detail in the next paragraph, due to the fact that this is a relatively new technique and the data treatment is complicated. An external FT-IR was available during some measurements. With this technique it is possible to measure concentrations of NO, NO_2, NH_3, HCN, N_2O, CO, CO_2 and C_xH_y continuously over the time. During the experiments performed with the external FT-IR the equipment was placed in series before the ECO Physics as shown in figure 4.2. Beside that, another diluter with a dilution rate of 1 to 110 was used during these measurements. The accuracy of this measurement technique depends on the performed calibration over a certain range.

4.2.2 In-situ FT-IR absorption spectroscopy

The in-situ Fourier transform infrared (FT-IR) absorption spectroscopy is used to measure the concentrations of NH_3, CO_2, CO, CH_4 and H_2O immediately above the fuel bed. This is done in order to measure the volatilisation of gaseous compounds from the fuel bed. The advantage of in-situ measurements compared to external measurement systems is that the concentrations are measured immediately in the hot section. Uncertainties caused by further reaction in time or during cooling down are not occurring. It is not possible to measure symmetrical molecules like O_2, H_2 and N_2 with the in-situ FT-IR system. Furthermore, it is not possible to measure NO, NO_2 and HCN, due to the low concentrations of these species. The way the in-situ FT-IR measurement equipment works, will be outlined briefly in this paragraph [Fleckl].

The FT-IR absorption spectroscopy is based on the fact that every infrared-active molecule absorbs photons at different wavenumbers. The FT-IR measurement equipment is shown in figure 4.3. By moving the mirror of the spectrometer, the frequencies are modulated optically, whereby the emission of the hot zones in the furnace have no influence.

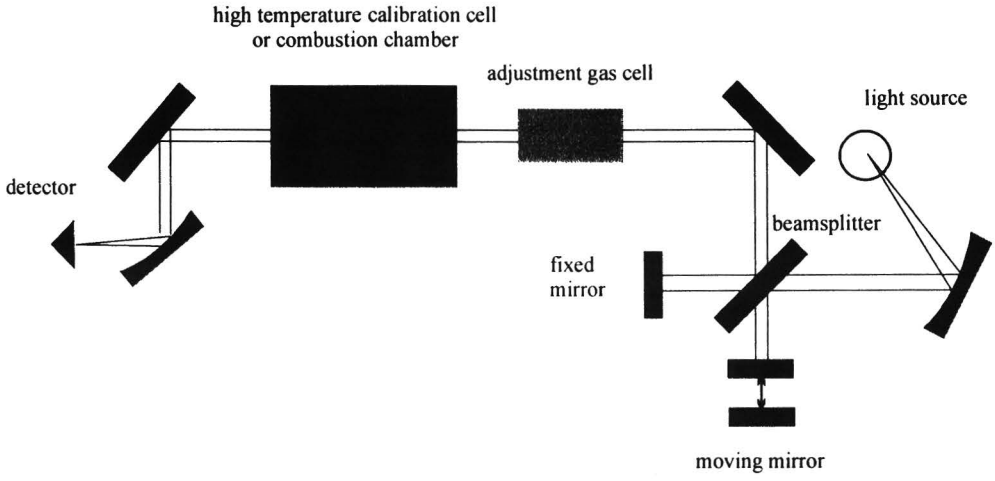

figure 4.3: Experimental set-up for the FT-IR absorption spectroscopy [Fleckl]

The data is collected in 16.7 seconds, whereby each spectrum is averaged over 20 scans. Three thermocouples are measuring the temperature over the path length, these are shown in figure 4.1.

The Beer-Lambert law describes the absorption of infrared radiation by a gas. The modified Beer-Lambert law is defined in equation 4.1.

$$A_m(\nu) = \alpha(\nu) \cdot n \cdot \ell \qquad (4\text{-}1)$$

Where $A_m(\upsilon)$ is the measured absorbance, $\alpha(\upsilon)$ the absorption coefficient, n the concentration of absorbing particles and ℓ the path length of radiation through the absorbing medium.

The absorption coefficient, $\alpha(\upsilon)$, of an infrared active gas component is dependent on the gas temperature, the gas concentration, the gas composition and the total pressure. Absorption coefficients as a function of these parameters were calculated by using the spectral database HITRAN/HITEMP and were measured during calibration measurements at a defined concentration and path length, ℓ.

By measuring the absorbance and temperature it is possible to calculate the concentration. By calculating the concentration in this way the concentration is in a range of 5-10% of the mean value for CH_4, CO and CO_2 and in a range of about 10-15% for water and NH_3.

Besides, an inaccuracy occurs, due to an appearing temperature gradient over the path length in the furnace. This gradient is measured with the thermocouples. The temperature dependence of the absorption is illustrated in the figure below.

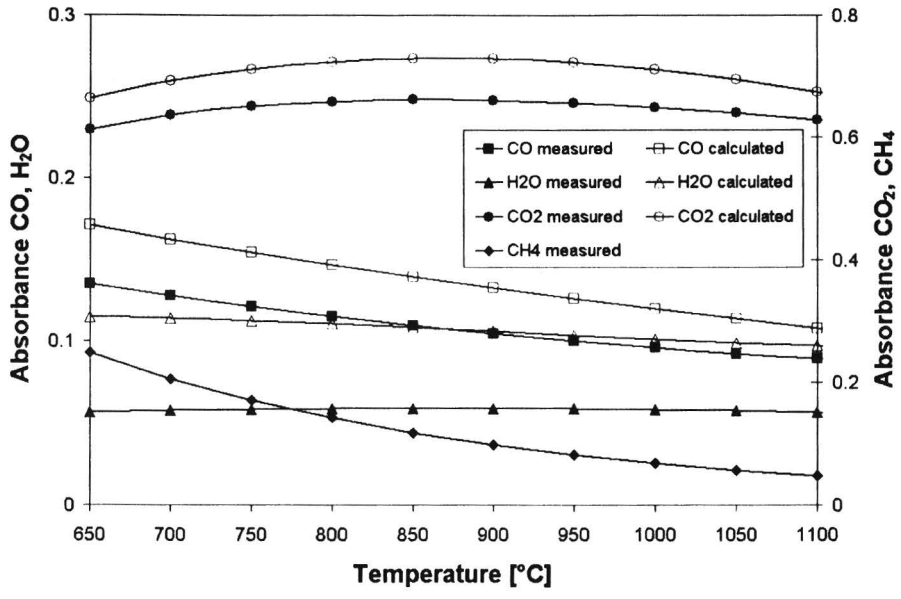

figure 4.4: ***Measured and calculated absorbance as a function of the temperature at a path length of 80 cm [Fleckl]***

With a temperature gradient of 20 degrees maximum this inaccuracy can be neglected compared to the range occurring on the mean value of the calculated concentration. Therefore, the absorbance and concentrations are assumed to be valid over the mean temperature in spite of the occurring temperature gradient.

A second inaccuracy occurs due to the fact that the exact path length is unknown due to the open side arms on the reactor. During some test runs Saphire windows are used to close the side arms in order to have a fixed path length and to measure the occurring inaccuracy. However, it is not possible to measure NH_3 with the Saphire windows. Therefore it is chosen to measure without the windows in spite of the inaccuracy involved.

4.3 Fuel type

Chipboard residues are applied as fuel during the experiments. This fuel is taken, because it is an important biomass fuel with a high concentration of nitrogen. The particle size of the chipboard used was in the range of 2.5-20 mm with a distribution in size as shown in figure 4.5.

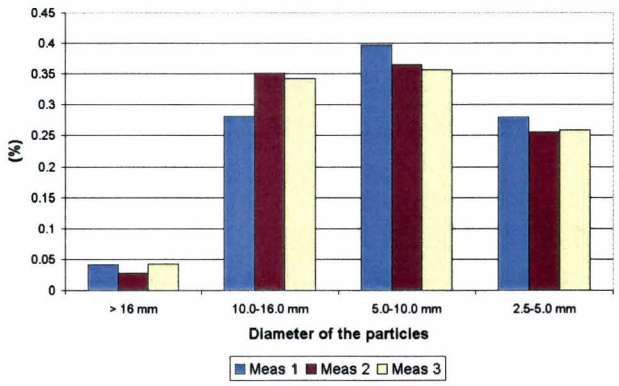

figure 4.5: distribution of the particle size

This distribution is determined experimentally by sieving the fuel. This process is repeated three times and the results are shown in figure 4-5. The particles smaller than 2.5 mm are not used. The mean particle diameter is 8.61 mm based on this distribution. The density of the applied fuel is determined experimentally by immersing a known mass of fuel and measuring the volume change of the water. The fuel was immersed for 10 seconds and was moved up and down to let the air go out of the fuel bed. The density of the fuel is averaged over the measured mass - volume fraction. The data measured is shown in the table below.

table 4-3: Density of the wet based fuel

	Mass (g)	*Volume change (10^{-3} l)*	*Density (kg/m^3)*
1	23.05	40	576
2	38.21	55	695
3	39.51	60	659

The mean density of the chipboard used during the experiments is found to be 643 kg/m^3. The fuel has no regular shape, but the bigger parts, > 10 mm, are rectangular and thin in height. The composition of the chipboard is shown in table 4-4.

table 4-4: composition of the chipboard

	Own analysis	*Weight-% [Keller]*
C	47	46.89
H	6	5.75
O	41.5 - 42.9	44.81
N	2.8 - 3.4	2.549
S	-	-
Ash	1.3 - 2.1	1.3
Moist	9 - 13	7
Volatiles	80	73.4

The reaction order and the stochiometric factor can be determined based on the composition of the chipboard. The reaction order is the amount of oxygen necessary for the complete combustion of 1 mole of chipboard, according to the following reaction:

$$C_x H_y O_z + \left(x + \frac{y}{4} - \frac{z}{2}\right) O_2 \rightarrow xCO_2 + \frac{y}{2} H_2O$$

The formula for chipboard is calculated easily by making use of the atomic mass and the composition of the chipboard [Keller, 1994]. This results in the following formula for the chipboard used: $CH_{1.532}O_{0.670}$. The stochiometric factor, λ is then 1.048 mole O_2/mole chipboard, which is equal to an air factor, L_{st} of 4.99 mole air/ mole chipboard [Weissinger, 2001]. Therefore, the combustion of chipboard can be approximated by a first-order reaction.

4.4 Data treatment

Data treatment for the FT-IR measurements is explained in the forgoing paragraph. As mentioned before, the data is logged every 16.7 seconds and is assumed to be the mean value over this time interval. For the other gas analysers the data have to be corrected due to the dilution rate, in order to know the concentration above the fuel bed. The data is logged every two seconds with Labview and it is assumed to be constant within this time step.

During devolatilization the total gas flow through the fuel bed increases compared to the inlet airflow. Based on the composition of the flue gas it is possible to estimate the increase of the airflow. Calculation of the volume flow is also necessary for calculating the total amount of species released, and the averaged amount of HCN and NH_3 released. The concentration of molecular nitrogen is assumed to be constant and can be calculated as follows:

$$[N_2] = 1 - [Sum\ of\ all\ species\ measured\ with\ the\ in\ situ\ FT\ IR] \qquad (4\text{-}2)$$

Calculating the nitrogen concentration on the way described above does neglect tar formation. The concentration of molecular nitrogen, $[N_2]$ is also described by the ratio of the nitrogen volume and the total volume. The nitrogen volume is defined in equation 4-3.

$$V_{N2} = \dot{V} \cdot (1 - [O_2]) \cdot \frac{1}{V_{spec}} \qquad (4\text{-}3)$$

Where $\dot{V}$ is the airflow, $[O_2]$ is the oxygen concentration, and V_{spec} is the molar volume of an ideal gas, which is 22.4 m^3/kmole. The total gas flow is equal to the ratio of the nitrogen volume divided through the nitrogen concentration as shown in equation 4-4.

$$V_{total} = \frac{V_{N_2}}{[N_2]} \qquad (4\text{-}4)$$

The total volume is expressed in mol/min. Calculation of the total amount released and calculation of the averaged amount released is possible, whereby the fluctuation in gas flow is taken into account. [Lans, 1998] estimated the gas flow on a similar way.

Correction of the measured temperature in the gas phase, due to radiation, is not necessary. A calculation of the temperature correction for a thermocouple in the gas phase proved this statement. This calculation is performed according to [Rindt, 1998], whereby the conduction is neglected due to the small diameter of the thermocouple.

The results obtained with the wet analyse method has to be treated to achieve the mean concentration in the flue gas [Keller, 1994]. The concentration of ammonia or hydrogen cyanide in the flue gas is calculated by making use of equation 4-5.

$$c_g = \frac{V_b \cdot c_b}{V_g} \qquad (4\text{-}5)$$

Where V_b is the volume of the solution in the bottle, V_g is the entire volume of the gas past through the bottles during the experiment and c is the concentration in the flue gas or bottle. The calculated concentration of NH_3 and HCN in the flue gas, c_g, is the averaged value of NH_3 and HCN released during the entire experiment.

5 Results of the measurements

The results of the measurements are discussed in two parts. The temperature profile in the bed is outlined first, followed by the influence of the airflow and oxygen concentration on the temperature. After that the release of species from the fuel bed is discussed in paragraph 5.2. In this part the different measurement techniques compared and the relation between the temperature profile and the emissions is discussed. This paragraph ends with a discussion of the influence of the airflow and oxygen concentration on the release of species. These results are compared to results obtained from literature. Finally, a short summary of the results deduced from the measurements will be made.

5.1 Temperature development

During the measurements two influence parameters are investigated. These are the airflow and the oxygen concentration. The influence of these parameters on the temperature development is outlined in the next paragraphs. Outlining the overall bed temperature development is done in paragraph 5.1.1.

5.1.1 Temperature profile in the bed

In the figure below the temperature profile in the bed is shown with the position of the thermocouples in the bed next to it, whereby thermocouple 2 is placed under the grate.

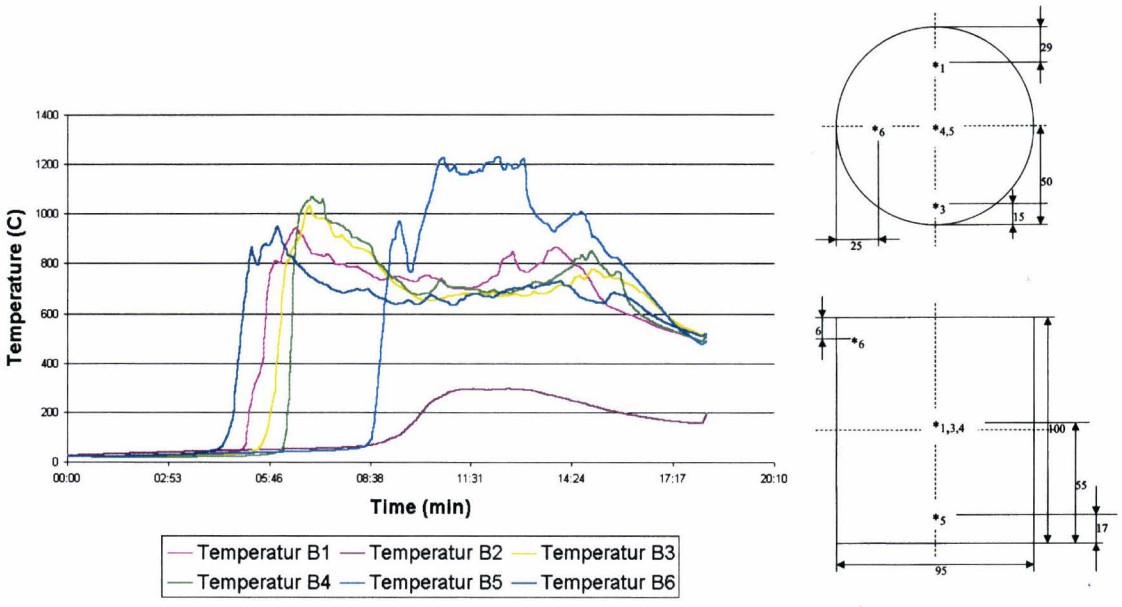

figure 5-1: ***The temperature in the bed for different thermocouples at an air flow of 25.4 l/min and an oxygen concentration of 21%.***

The temperature development in the bed, shown in figure 5-1, is representative for all measurements. The fuel first ignites at the location of thermocouple 6, followed by thermocouple 1, 3 and 4 and ends with the ignition of thermocouple 5. So, the ignition front propagates downwards through the bed.

The thermocouples 1, 3 and 4 are positioned on the same height in the bed. Figure 5-1 shows that a horizontal temperature gradient is occurring in the bed. This gradient is not caused by an instability of the bed, because the measured pressure drop over the bed is in the same order of magnitude as the calculated pressure drop [VDI, Le 1]. Therefore, it is assumed that the gradient is caused by the lower resistance at the wall side of the pot furnace. Optimisation by changing the particle size did not result in better results.

The measured temperature as function of time was reproducible over the range of parameters measured. As an example of the reproducibility of the temperature in time, the mean temperature of thermocouple 6 with a 95% confidence interval is shown in figure 5-2. Each mean temperature profile is calculated from at least three to four measurements.

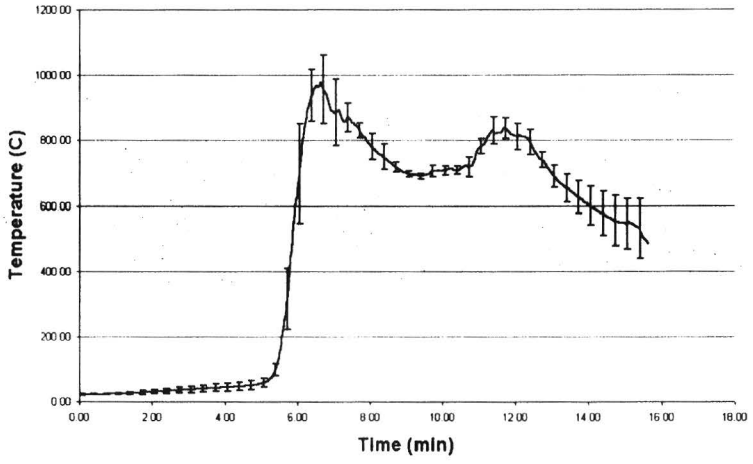

figure 5-2: ***Reproducibility of the temperature as function of time at a mean airflow of 40 l/min and an oxygen concentration of 21 % at thermocouple 6.***

The temperature profile, illustrated in figure 5-2, starts with a rise in temperature due to the ignition of the fuel bed. The ignition front propagates downwards through the bed and the thermocouple enters the gas phase. This results in a decrease of temperature due to the fact that radiation and convection are heating the thermocouple. At the end of the measurement a rise in temperature occurs again due to the start of the char combustion, which occurs at higher temperatures than the gasification phase. This is illustrated by thermocouple 5, which is positioned in the char layer or just above it (figure 5-1).

The maximum temperature, the propagation velocity and the ignition time varies depending on the airflow and the oxygen concentration. This will be discussed in the next paragraphs.

5.1.2 Influence of the airflow on the temperature

The fact that the temperature depends on the airflow is illustrated in figure 5-3 for the thermocouples 6, 4 and 5.

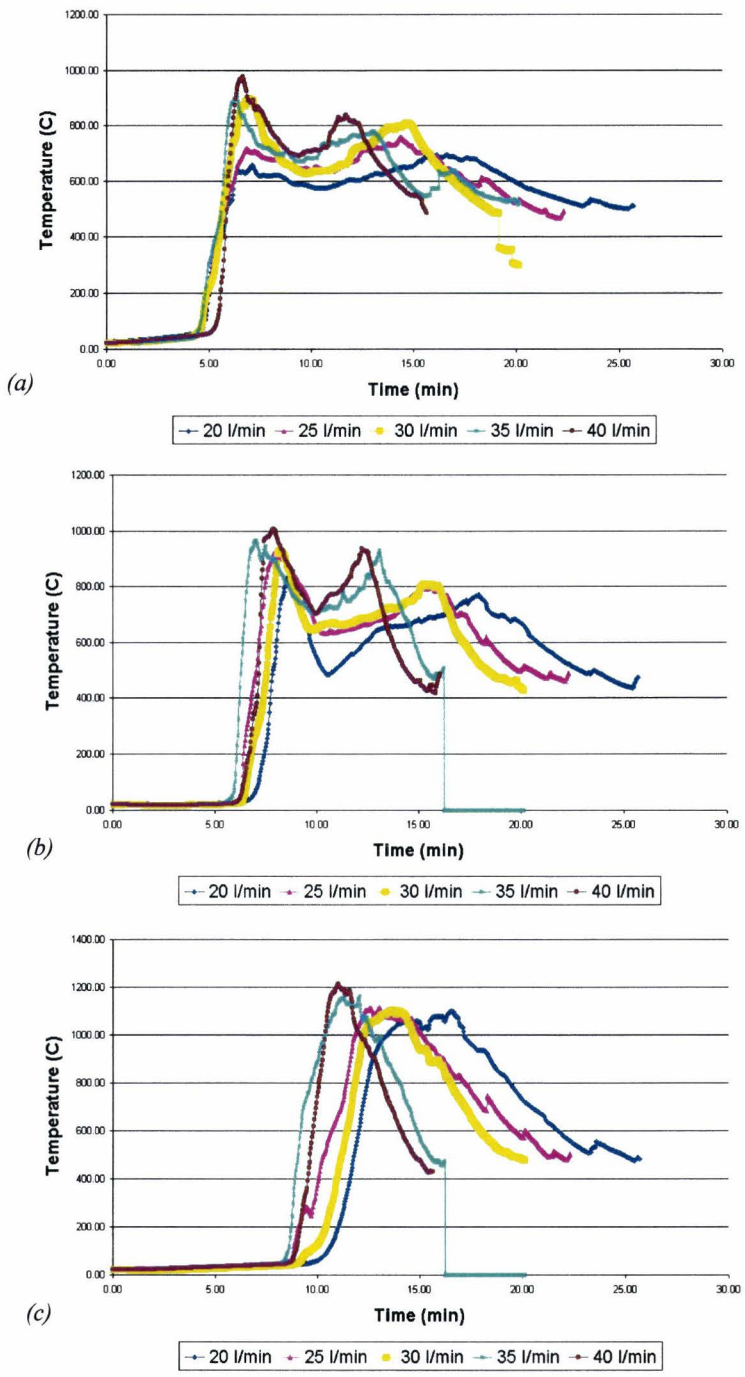

figure 5-3: ***Mean temperature development at a certain thermocouple as function of the airflow at an oxygen concentration of 21% (based on three to four measurements), (a) Temperature in time at thermocouple 6, (b) Temperature in time at thermocouple 4, (c) Temperature in time at thermocouple 5.***

In figure 5-3a it is shown that the airflow has a slight influence on the ignition time; the time it takes before ignition starts. This implies that convection and conduction are negligible compared to the heating up by radiation in the upper layer. Neglecting convection can be explained by the fact that if the layer is really thin the surface of convection becomes small. This is illustrated in the figure below.

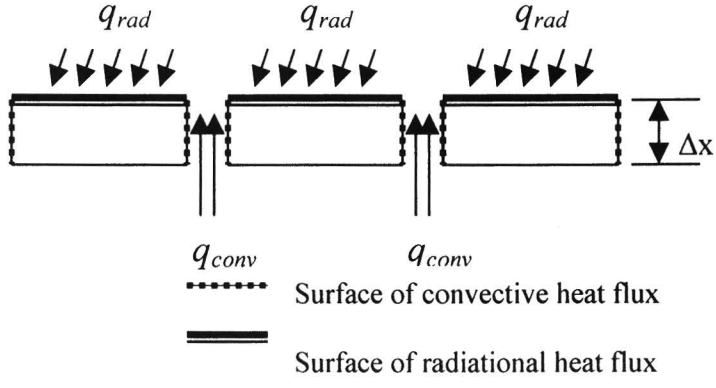

figure 5-4: ***Surface of convection compared to radiation.***

If the surface over which the convection takes place becomes small ($\Delta x \rightarrow 0$) the in influence of convection is negligible compared to radiation. In figure 5-3 a steep gradient in the bed temperature is visualised. This gradient occurs due to slow diffusivity and therefore it's allowed to neglect the conductive heat transfer. The fuel bed is heated up by radiation and the ignition time is independent of the airflow at the top of the fuel bed.

A difference in front propagation velocity is measured over the whole legth of the bed between thermocouple 5 and 6. Thermocouple 5 ignites in the following order: 35, 40, 25,30 and 20 l/min. The reaction front propagation velocity is derived from the distance between thermocouple 5 and 6 and the time shift between them at a temperature of 200, 400 and 600 °C. In figure 5-5 the reaction front propagation as function of the air flow is illustrated.

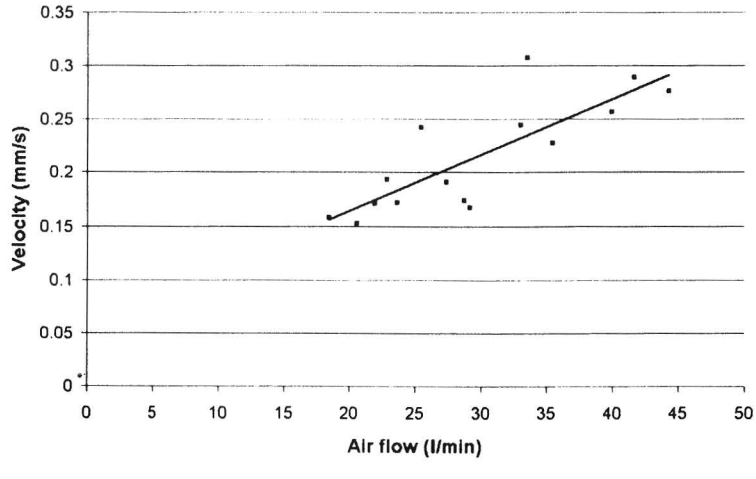

figure 5-5: ***Reaction front propagation velocity as function of the airflow, derived from the distance between thermocouple 5 and 6 and the time shift between them to reach a certain temperature.***

In the figure above, it is shown that a rise in airflow results in a rise of the reaction front propagation velocity. This rise in front propagation velocity is in accordance with the literature [Saastamoinen, 1999] over the range of airflows measured. [Saastamoinen, 1999] found a maximum for the reaction front propagation velocity at an airflow of 0.22 $kgm^{-2}s^{-1}$. This maximum is found for higher airflows than measured during these experiments (40 l/min=0.0258 $kgm^{-2}s^{-1}$). Therefore, a rise in airflow results in a rise of the propagation velocity. The measured ignition speed is in the same order of magnitude as measured by [Saastamoinen, 1999], who measured a front propagation velocity of 0.3 – 0.4 mm/s.

The results obtained from measurements show a significant influence of the airflow on the combustion time (figure 5-3). An increase in airflow results in a shorter combustion time, which is in accordance with literature [Van de Geijn, 2000]. Beside that, the maximum bed temperature decreases at a lower airflow, which is in accordance with [Lans, 1998b] and not with [Saastamoinen, 1999]. According to [Saastamoinen, 1999] a decrease of the maximum bed temperature will occur at a higher airflow due to the higher front propagation velocity. This difference can be explained due to the fact that the measurements are performed at lower airflows compared to the measurements performed by [Saastamoinen, 1999]. It is likely that an optimum in bed temperature will occur for a certain airflow. After a certain airflow, a further increase will cool down the temperature in the bed.

5.1.3 Influence of the oxygen concentration on the temperature

The temperature dependency of the oxygen concentration is illustrated in figure 5-6 for thermocouples 6, 4 and 5.

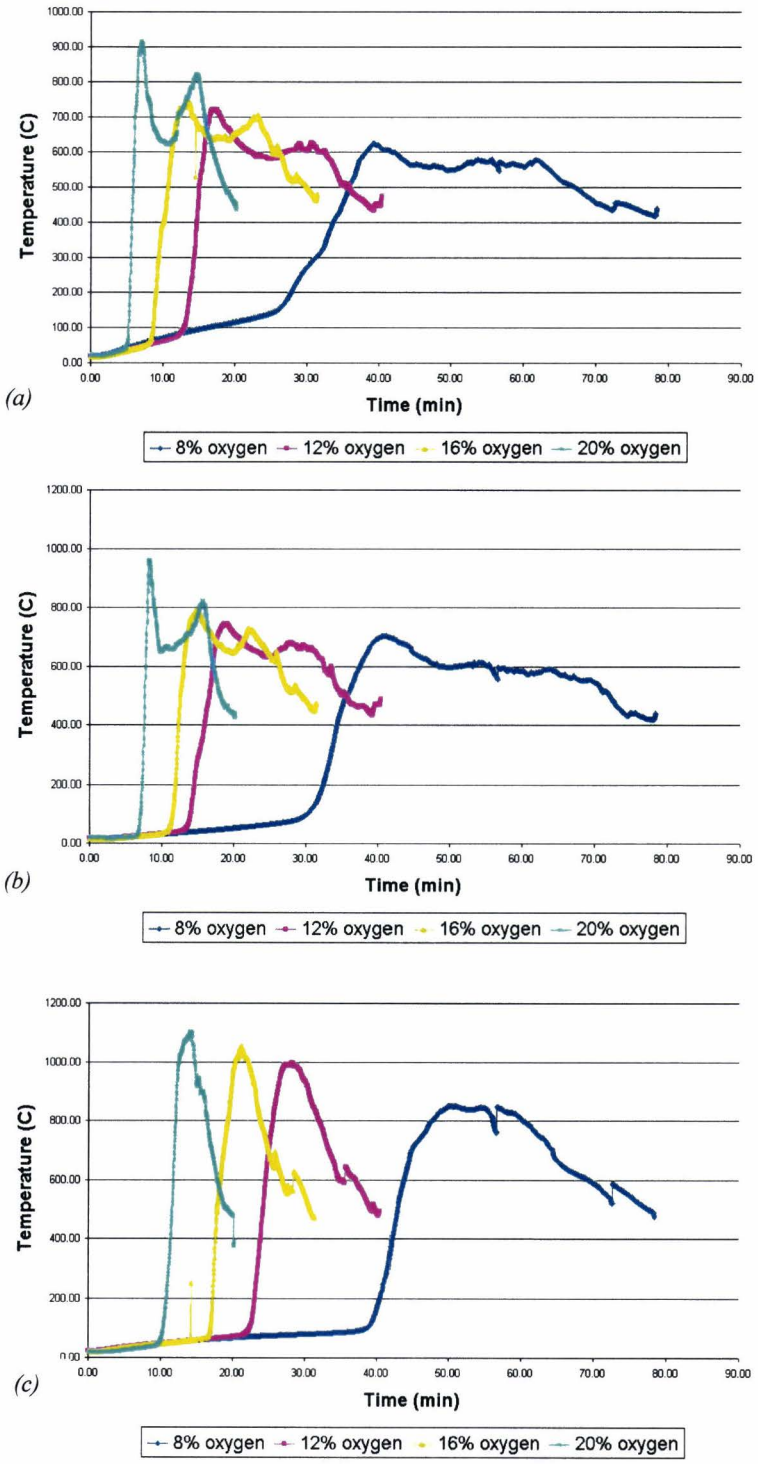

figure 5-6: ***Mean temperature development at a certain thermocouple as function of the oxygen concentration at a mean airflow of 30 l/min (based on three to four measurements), (a) Temperature in time at thermocouple 6, (b) Temperature in time at thermocouple 4, (c) Temperature in time at thermocouple 5.***

An increase in oxygen concentration results in an earlier ignition, shorter combustion time and a higher maximum bed temperature, which is illustrated in the figure above. An increase of the reaction velocity and an increase of the heat of reaction, and thus a

higher maximum bed temperature, corresponds to the literature [Van de Geijn 2000]. The reaction front propagation velocity as function of the oxygen concentration is shown in figure 5-7.

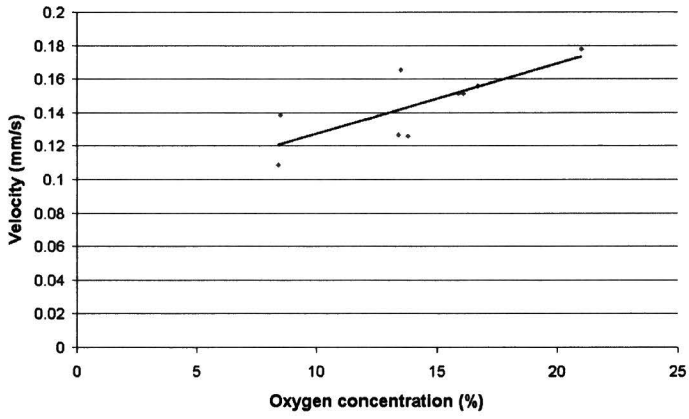

figure 5-7: ***Reaction front propagation velocity as function of the oxygen concentration, derived from the distance between thermocouple 5 and 6 at the time shift between them.***

The propagation velocity is derived in the same way as for the airflow. By comparing the influence of the oxygen concentration (figure 5-7) and the airflow (figure 5-5) on the propagation velocity, it is clear that the influence of the oxygen concentration is much smaller than the influence of the airflow. Care has to be taken, because the influence of the air flow is investigated at an oxygen concentration of 20%.

5.2 Release of species from the fuel bed

During the measurements, different equipment is used for measuring gaseous species as outlined in chapter 4. A comparison between the different measurement techniques will be outlined first, followed by the relation between the temperature profile and the release of species. The paragraph ends with the influence of the airflow and the oxygen concentration on the emission of species from the fuel bed.

5.2.1 Comparison between the different measurement equipment

In this paragraph the different measurement techniques are compared. The wet analysis method will be compared with the in-situ and the external FT-IR concerning the release of NH_3 and HCN from the fuel bed. Furthermore, a comparison is made between the external FT-IR and the Eco Physics concerning the NO, NO_2 and the NO_x. At the end the CO, CO_2, CH_4 and H_2O emissions measured, will be compared for the in-situ and the external FT-IR.

Wet analysis method compared to the in-situ and the external FT-IR

As described in chapter 4.4, the mean release of NH_3 is calculated for the external and in-situ FT-IR. This means that the release is averaged over the volume. The average release of NH_3 for different oxygen concentrations is shown in figure 5-8 for the three different measurement techniques.

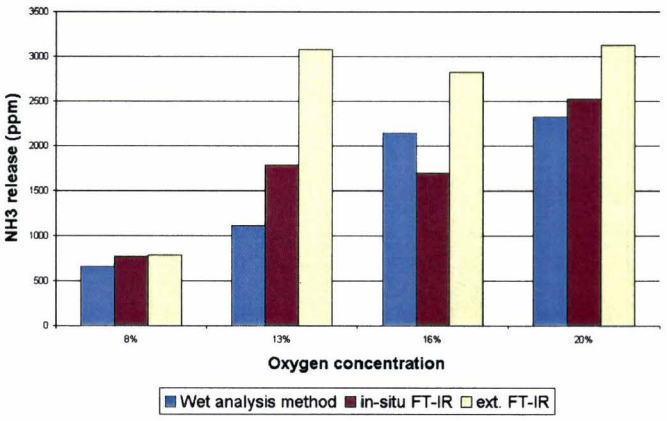

figure 5-8: ***Mean release of NH_3 measured with the wet analysis method, the in-situ FT-IR, and the external FT-IR at different oxygen concentrations and a mean airflow of 30 l/min.***

From the figure above, it is clear that the external FT-IR measures higher values of NH_3 compared to the other two measurement techniques. Beside that the release of NH_3 shows a time shift between the data collected with the external FT-IR and the in-situ FT-IR, which is illustrated in the figure below.

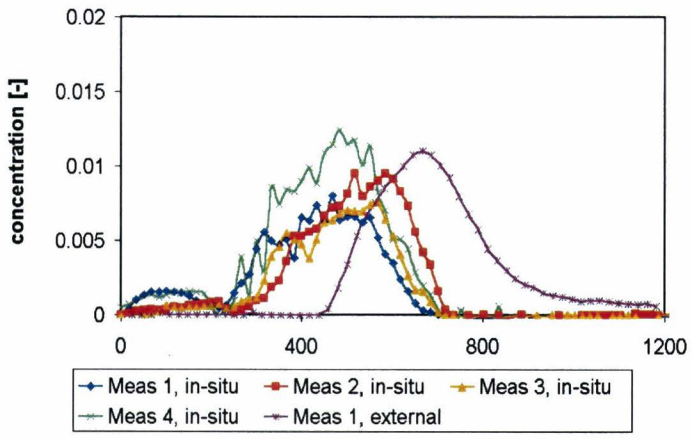

figure 5-9: ***NH_3 release measured with the in-situ and the external FT-IR during different test runs. Test runs are performed at a mean airflow of 30 l/min and an oxygen concentration of 21%***

Due to these differences the data collected with the external FT-IR are not used for deducing trends. The data collected with the in-situ FT-IR is well comparable to the data collected with the wet analysis method. This shows that the in-situ measurements are plausible and that the accuracy is within the ranges of other standard techniques. Therefore, the in-situ FT-IR is only used to deduce trends concerning the release of ammonia. Besides that, the method has the advantage of a time dependent release instead of a mean value over the whole measurement.

External FT-IR compared to the Eco Physics

During some measurements an external FT-IR was positioned in series between the fuel bed and the Eco Physics. The measured concentration of nitrogen species during the same test run is shown in figure 5-10.

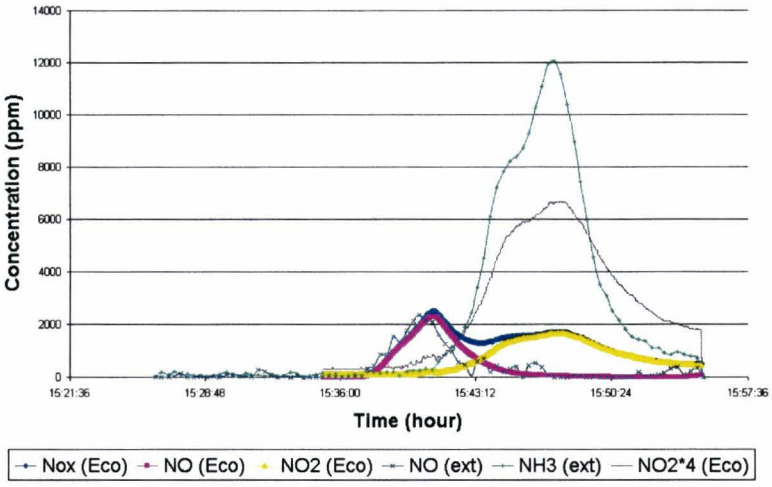

figure 5-10: ***Nitrogen release measured with the external FT-IR in series and with the Eco Physics during the same test run at an air flow of 25.5 l/min and an oxygen concentration of 21%.***

For clarity, the data from the N_2O and HCN emissions, measured with the external FT-IR, are not shown because the concentrations of those species are negligible. The figure above shows that the NO concentration measured with the Eco Physics is the same as with the external FT-IR. This means that there are no further reactions occurring with NO after the external FT-IR at a dilution rate of 1 to 110.

However, questions do arise concerning the NO_2 emissions. There is no NO_2 release measured with the external FT-IR in contrast with the Eco Physics. Furthermore, NO_2 is also not expected from literature. But a correlation between the NO_2 reading with the Eco Physics analyser and the NH_3 reading of the external FT-IR can be made. This is illustrated by multiplying the NO_2 concentration by four. It seems that the same fluctuation in NO_2 emissions occurs as for NH_3 (figure 5-10). This means that it is probable that further reactions of NH_3 to NO_2 are occurring in the measurement equipment. Catalytic reactions of NH_3, with other species in the flue gas, at the refined steel in the convertor at a temperature of 450°C are likely to appear. This means that the NO_2 reading of the Eco Physic analyser increases with a release of NH_3 and that the NO_2 is not released directly from the fuel bed.

The concentration of NO, NO_2 and NO_x, measured with the Eco Physics, diverts for the test runs with the external FT-IR in series and without. This is illustrated in figure 5-11.

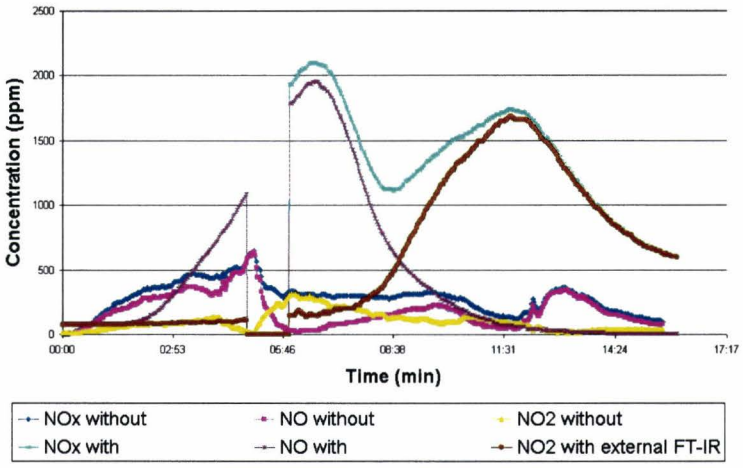

figure 5-11: ***Concentration of NO, NO_2 and NO_x, measured with the Eco Physics during two different test runs, whereby one test run is performed with an external FT-IR in series and one without (setting with external FT-IR: airflow of 38.6 l/min and oxygen conc. of 21%, setting without the external FT-IR: 44.2 l/min and oxygen conc. of 21%).***

In the figure above, it is shown clearly that the concentration, measured during the test runs with the external FT-IR in series, is much higher than during the test runs without. Beside that a clear time shift occurs in the release of nitrogen species, which could be caused by a longer residence time in measurement system. Differences caused by unstable dilution rates seem to have no influence, because the dilution rates are checked, during the test runs, by measuring the oxygen content in the air at the dilution settings. A possible reason for the diversion is that there are occurring further reactions during the test runs without the external FT-IR, due to the lower dilution rate of 1 to 10. Beside that, a different dilution rate can result in a difference in residence time, which can have his influence on the concentrations.

The results obtained during the test runs with the external FT-IR are describing a parabolic release of nitrogen species (figure 5-11), which seems to be incorrect. Perhaps this occurs due to re-mixing effects, according to a perfectly stirred reactor, in the measurement cell. This is shown by the peak signal assimilating a gaussion distribution function.

Furthermore, the amount measured with the external FT-IR is much higher than the amount found in literature. [Keller, 1994] found a maximum release of 400 ppm NO, which is in the range of the data collected with the Eco Physics. Due to these reasons, the NO data of the external FT-IR are not used to deduce a trend for the influence of the airflow and the oxygen concentration on the release of species from the fuel bed.

In-situ FT-IR compared to the external FT-IR

The emissions of NH_3, H_2O, CO, CO_2, and CH_4 are measured with both measuring techniques. A comparison of NH_3 and HCN is already made in the paragraph before. In the figure below the emissions of CO, CO_2, CH_4, and H_2O are illustrated for different test runs at fixed measuring conditions.

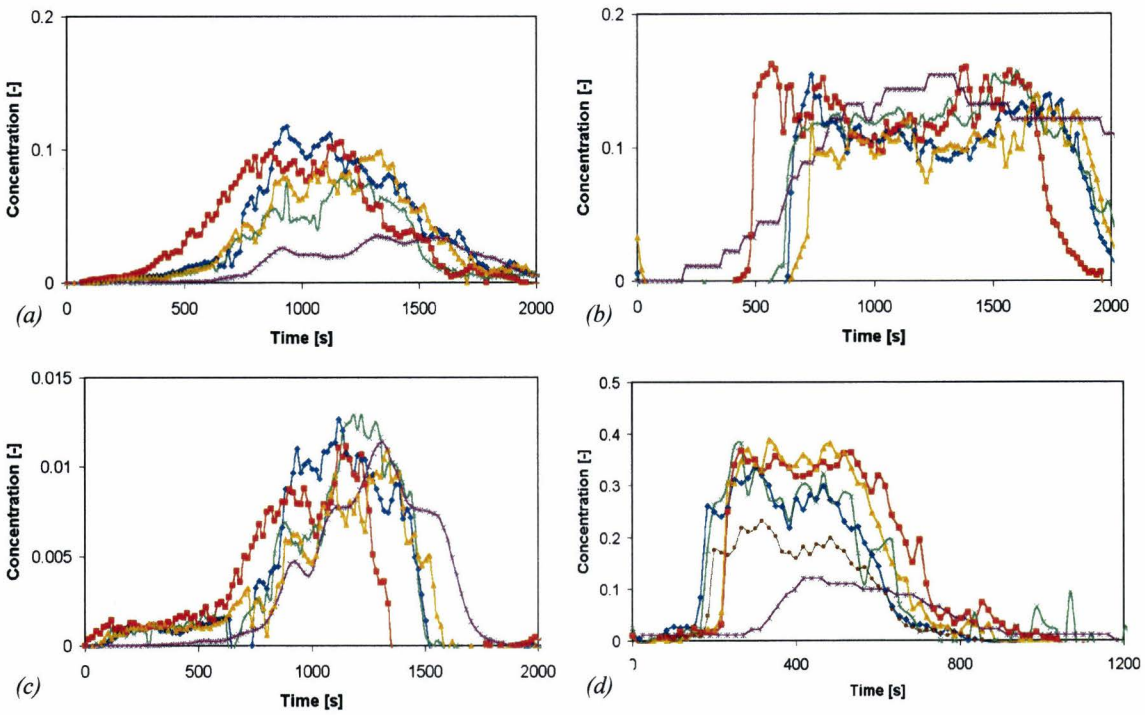

blue = *Measurement 1; in-situ FT-IR*
purple = *Measurement 1; external FT-IR*
red = *Measurement 2; in-situ FT-IR*
orange = *Measurement 3; in-situ FT-IR*
green = *Measurement 4; in-situ FT-IR with Saphire windows*

figure 5-12: ***(a) Emission of CO, (b) emission of CO_2,(c) emission of CH_4 and (d) emission of H_2O at different test runs. Test runs are performed at a mean airflow of 30 l/min and a mean oxygen concentration of 13%.***

The reproducibility of the measurements performed with the in-situ FT-IR is clear from the figure above. The data collected with the in-situ FT-IR is in the same range for the measurements with and without the external FT-IR. This means that the external FT-IR does not influence the in-situ FT-IR.

Measurement 4 is performed with the Saphire windows in order to check the influence of the unknown path length as described in chapter 4.2.2. The results obtained confirm the decision of measuring without the Saphire windows, which made it possible to measure NH_3 with the in-situ FT-IR.

The data collected with the external FT-IR is in the same range of the data collected with the in-situ FT-IR for CO_2 and CH_4. However, the concentration of H_2O and CO measured with the external FT-IR is much lower than the concentration measured with the in-situ FT-IR. Taking into account the inaccuracy of the in-situ FT-IR does not solve the difference. Maybe, the difference is caused by further reactions in the gas phase, which is in contradiction with the fact that the CO_2 concentration is in the same range. Therefore, only the data collected with the in-situ FT-IR will be used to

evaluate the influence of the airflow and oxygen concentration on the release of species from the fuel bed.

5.2.2 Relation between the temperature profile and the emission of species

The release of species compared to the temperature profile is illustrated for a mean airflow of 30 l/min in figure 5-13.

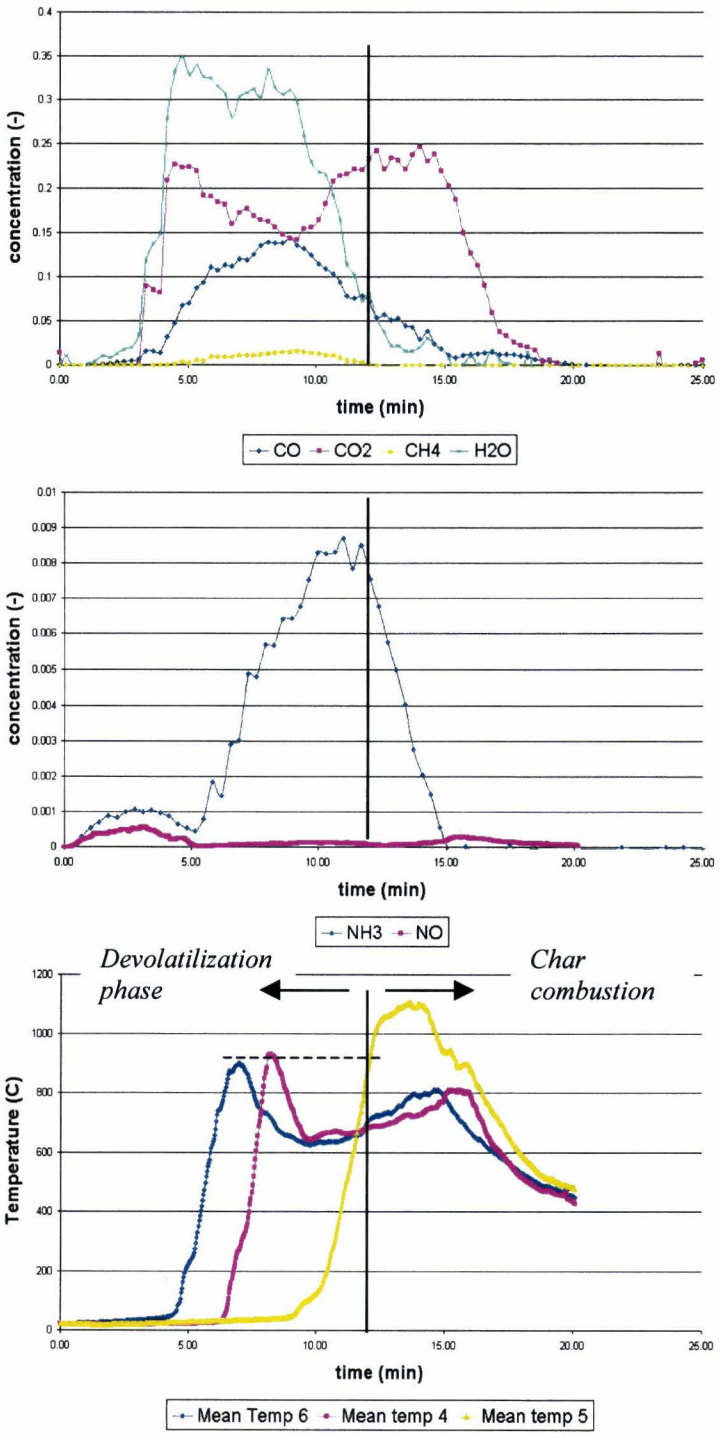

figure 5-13: ***(a) Release of CO, CO_2, and CH_4, (b) release of NH_3 and NO in time compared to (c) the temperature profile in the bed for a mean airflow of 30 l/min and an oxygen concentration of 21%***

It is assumed that the devolatilization phase changes to the char combustion, burnout phase, as thermocouple 5 reaches a temperature higher than the maximum bed temperature occurred so far. figure 5-13 shows that the release of H_2O and CO_2 starts immediately after ignition followed by CO and NH_3. Some water vapour is already released due to the drying process. Before ignition, a small increase in the emission of NH_3 and NO occurs. An explanation for this peak is not found, but it can be assumed that this occurs due to highly volatile components of the fuel. The release of HCN and N_2O is negligible and is not shown in figure 5-13. Ammonia, NH_3 is the main nitrogen component released over the range of airflow's and concentrations measured.

During char combustion a clear drop occurs in the concentration of NH_3 and H_2O. This is in accordance with [Lans], who found that ammonia is only released during devolatilization and not during char burnout. On the other hand, a slight increase of the NO concentration occurs due to more oxygen present during char combustion, which is confirmed by [Hill, 2000]. According to [Hill, 2000], nitrogen-containing species will be reduced to N_2 in fuel-rich regions. The release of CO and CH_4 decreases slowly during char combustion. However, the emission of CO_2 rises again. This seems to be caused by the oxygen rich conditions during char burnout. The effects of the temperature on the release of species described above, are all in accordance with the results obtained by [Lans].

5.2.3 Influence of the airflow on the release of species

The influence of the airflow on the release of CO_2 is illustrated in figure 5-14.

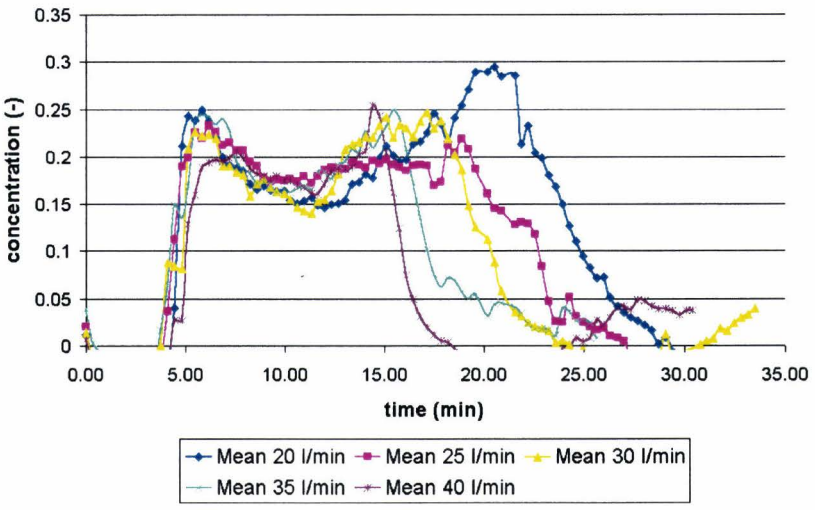

figure 5-14: ***Release of CO_2 as function of the airflow at an oxygen concentration of 21%***

The airflow has a slight influence on the starting point of the release of CO_2, which is in accordance with the fact that the airflow has a negligible influence on the ignition time. An influence occurs during char combustion, where the amount and the period of release increase for a lower airflow. This effect agrees with the results obtained in paragraph 5.1.2, where it is found that the char burnout starts little later and takes a longer time for a lower airflow. The same effect of the airflow on the release of CO, CH_4, NH_3 and H_2O is found. The release of those species as function of the airflow is illustrated in appendix A.3.

The CO concentration was about 12-14 vol%, the CO_2 concentration about 20 vol%, the CH_4 concentration about 1.5 vol% and the H_2O concentration was about 30-35 vol% over the range of air flows measured. These values are in the same order of magnitude as the results obtained by [Lans], who performed experiments in the same range of airflow and oxygen concentration with straw as fuel[1].

The total amount of NH_3, CO, CO_2, H_2O and CH_4 is calculated by multiplying the concentration with the gas volume, which is dependent of the release of species (see chapter 4.4). In figure 5-15, the total amount released as a function of the airflow is illustrated.

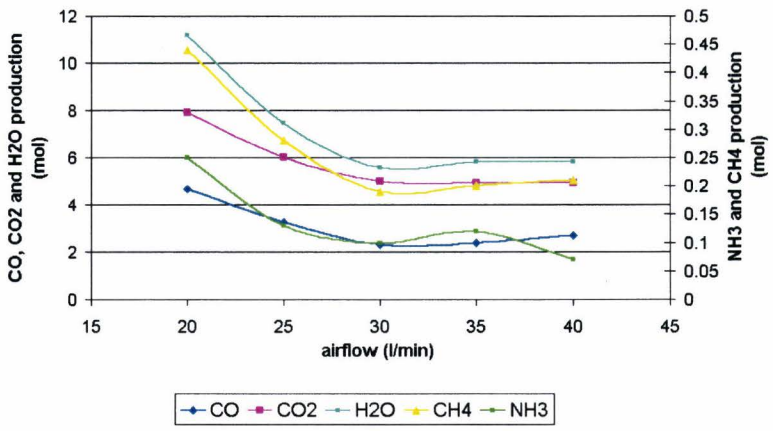

figure 5-15: ***Total amount of NH_3, CO, CO_2, H_2O and CH_4 released during different test runs as function of the airflow at an oxygen concentration of 21%***

The effect of the airflow on the release of species is clear from the figure; an increase in airflow results in a lower conversion. Tar is not measured during the test runs, but it is probable that the production of tar is higher for an increasing airflow. The lower conversion of fuel-N to NH_3, is also found by [Lans]. At lower airflows, the conversion of fuel-N to molecular nitrogen is getting more important, because molecular nitrogen is not a pollutant for the environment. Therefore, the furnaces should not operate with too low airflows, because the release of NH_3 and NO seems to increase during the devolatilization phase.

A higher conversion at a lower airflow seems to be in contradiction with the higher maximum bed temperature for an increasing airflow. However, this effect could be explained by the change in combustion regime from smouldering to flaming conditions. According to [Bilbao], a variation in oxygen concentration can lead to a change in the combustion regime from smouldering, heterogeneous reactions to flaming conditions, homogeneous reactions. Smouldering conditions, low oxygen concentration, typically yield to a higher conversion of wood to gases than under flaming conditions, though at a lower rate. Perhaps, this effect occurs at the low airflows, where diffusion seems to be the reaction controlling parameter.

[1] CO conc. of 10-20%, CO_2 conc. of 15-17%, C_xH_y conc. of 1.5 vol% and H_2O conc. of 20-30 vol% [Lans]

5.2.4 Influence of the oxygen concentration on the emission of species

The influence of the oxygen concentration on the release of NH_3 is shown in figure 5-16.

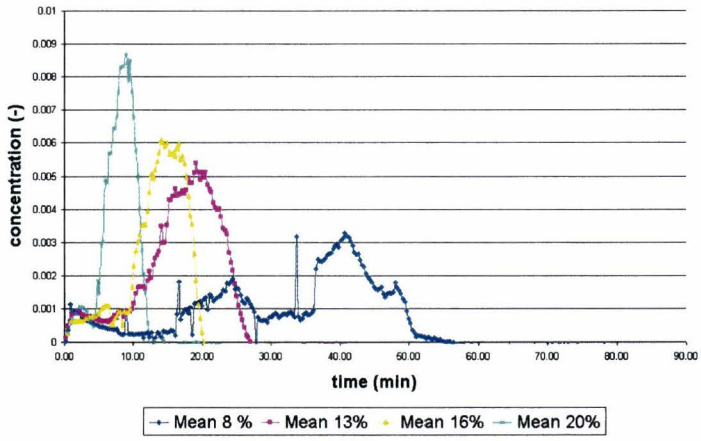

figure 5-16: ***Release of NH_3 as function of the oxygen concentration at an air flow of 30 l/min***

From the figure above the following conclusions can be made:

1. An increase of the oxygen concentration results in an earlier starting point at which NH_3 is released.
2. An increase of the oxygen concentration results in a higher maximum concentration of NH_3.
3. An increase of the oxygen concentration results in a shorter period in which NH_3 is released.

These effects are also found for CO, CO_2, H_2O, and CH_4 and confirm the influence of the oxygen concentration on the temperature profile in the bed. An earlier release confirms an earlier ignition, a higher maximum concentration confirms a higher maximum bed temperature and a shorter period at which the release occurs confirms a shorter combustion time for an increasing oxygen concentration. The release of the other species: CO, CO_2, H_2O, and CH_4 as a function of the oxygen concentration is illustrated in appendix A.3. Data of the NO emissions is hard to interpret, because the starting point of release is the same for every oxygen concentration. Beside that the results are in contradiction with the results from literature [Van de Geijn, 2000]. According to [Van de Geijn, 2000], an increase in oxygen concentration leads to an increase in the conversion of fuel-N to NO. Due to these differences, the data obtained with the Eco Physics is not used to deduce a trend for the release of NO.

The total amount of NH_3, CO, CO_2, H_2O and CH_4 is calculated by multiplying the concentration with the gas volume, which is dependent on the release of species (see chapter 4.4). In figure 5-17, the total amount released as function of the oxygen concentration is illustrated.

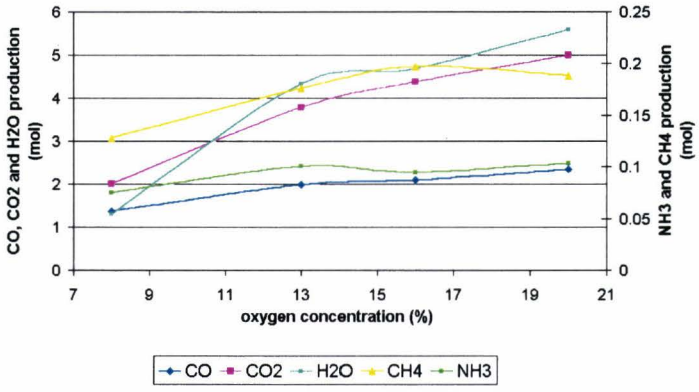

figure 5-17: ***Total amount of NH_3, CO, CO_2, H_2O and CH_4 released during different test runs as function of the oxygen concentration (Watch out: primary and secondary axis)***

An increase in the oxygen concentration results in an increase for CO, CO_2, H_2O, and NH_3, as shown in the figure above. The release of CH_4 shows a maximum for an oxygen concentration of 16%. Tar is not measured during the test runs, but it is assumable that the tar production is higher for a lower oxygen concentration.

A higher conversion of biomass is the result of an increase in oxygen concentration, which is in contradiction to the literature [Bilbao]. As mentioned before, a variation in oxygen concentration can lead to a change in the combustion regime from smouldering, heterogeneous reactions to flaming conditions, homogeneous reactions. However, this influence is not found for the measurements performed during this investigation. Therefore, all the measurements seem to be performed at flaming conditions.

5.3 Summary of the results obtained from measurements

A clear distinguish can be made between the species released during devolatilization phase and the char combustion phase. Ammonia and water vapour are released during the devolatilization phase and the emission of CO_2 and NO increases during char burnout.

The effects of the airflow and the oxygen concentration on the temperature and the emission of species are listed in Table 5-1. The trends are deduced over the range of airflows (20 – 40 l/min) measured, at an oxygen concentration of 21%, and over the range of oxygen concentrations (8 – 20 %) measured, at a mean airflow of 30 l/min.

Table 5-1: The influence of the airflow and the oxygen concentration on the temperature and the emission of species

Influence parameter	*Influence on the temperature*	*Influence on the emission of species*
An increase of the airflow results in	no influence on the ignition time	negligible influence on the start point of emission
	a higher reaction front propagation velocity	a shorter release of species
	a shorter combustion time	
	higher maximum bed temperature	a lower conversion
An increase of the oxygen concentration results in	an earlier ignition	an earlier release
	shorter combustion time	a shorter period at which emissions occur
	a higher reaction front propagation velocity	
	a higher maximum bed temperature	a higher maximum concentration released

Due to the diversity of the data obtained with the different measurement techniques, it is chosen to deduce only trends with the data collected. Further test runs are necessary to clarify the differences, which would make it possible to determine the influence of the airflow and oxygen concentration on the amount of species released.

6 Results of the model

The conversion of fuel is analysed by making use of the model presented in chapter 3. A sensitivity analysis of the model is performed for numerical parameters: the amount of layers and the time step. After that, the model is compared to the measurements, whereby differences between the calculated and measured data are indicated. Furthermore, suggestions to improve the model are made. However, the model is first used to show a distinct ignition front in the bed.

6.1 Ignition front propagation

As discussed in chapter 5 an ignition front propagates through the bed. Before measuring, calculations are performed in order to show the existence of a distinct ignition front over the packed bed. The results of the pot furnace can be used to simulate a grate furnace if this distinct ignition front is found.

The calculations, in order to determine the existence of a propagating ignition front, are performed with the bed divided in 50 layers and a time step of 0.01s. Results of the calculation are illustrated in the figure 6-1.

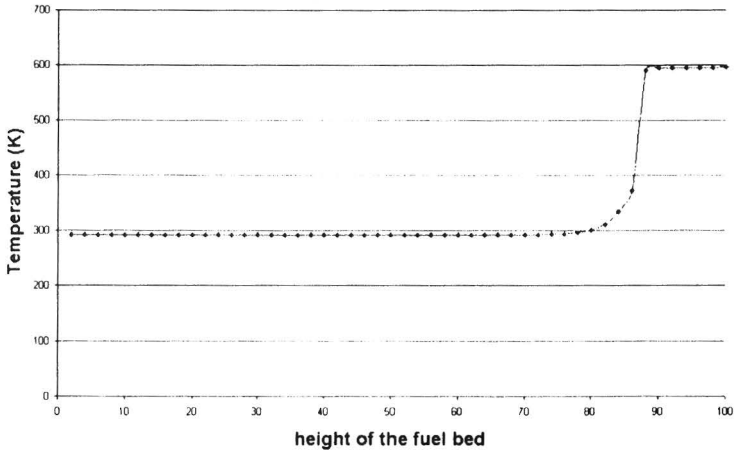

figure 6-1: ***Calculated temperature profile in the bed at t = 500s as function of the height in the bed. Calculation is performed with the model as described in chapter 3. (Amount of layers = 50, dt = 0.01 s)***

A steep gradient in temperature is calculated over the bed as shown in figure 6-1. This confirms the clear separation between the heating zone and the combustion zone, which is also found by [Gort, 1995].

6.2 Calculated conversion of biomass

Parameters of numerical influence are discussed in this paragraph. The influence is investigated for only two values. Therefore, it is not possible to show the range for which the influence on the conversion or temperature is negligible.

During calculation the mass of the layer is assumed to be zero as soon as it is lower than 10^{-100} g. This is necessary because of Matlab, for which an infinitesimal mass is still not equal to zero. Calculation with a mass limitation of 10^{-10}g showed a clear influence; a quicker conversion and a lower maximum bed temperature.

The model is tested for two different time and place steps. The results of the calculated temperature profile in the upper layer of the bed are shown in figure 6-2.

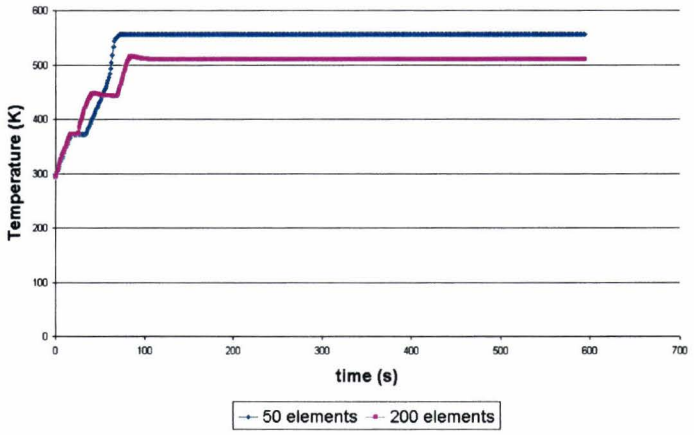

figure 6-2: ***Calculated temperature profile for an airflow of 20 l/min at different settings in time and place. One calculation is performed with 50 layers and a time step of 0.01s and the other is performed with 200 layers and a time step of 0.001s***

Furthermore, the results of the calculated mass decrease are shown in figure 6-3.

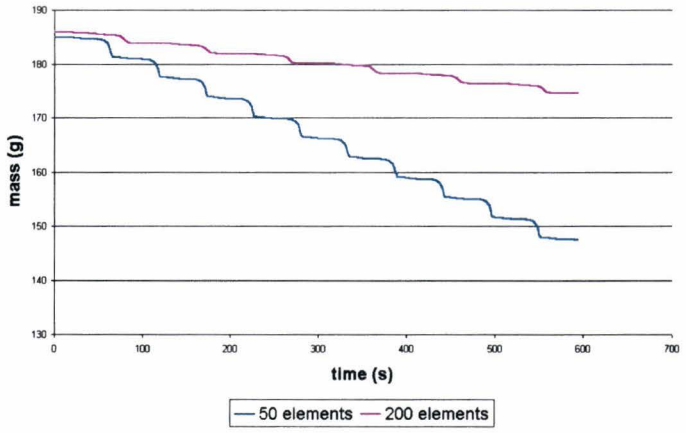

figure 6-3: ***Calculated mass decrease for an airflow of 20 l/min at different settings in time and place. One calculation is performed with 50 layers and a time step of 0.01s and the other is performed with 200 layers and a time step of 0.001s***

The calculation, performed with the bed divided into 50 layers, shows a numerical instability for the mass decrease. At this setting the mass decrease shows a gradual decrease in mass. This is caused by the physically incorrect way of modelling the water vaporisation. If the water content of a layer is too high the water vaporisation is not finished when the layer above has burned out, which causes an intermittent

combustion. Therefore, the amount of layers has to be chosen such that the ignition front propagates continuously through the bed.

Calculation, with the bed divided into 200 layers, showed a negligible influence on the mass decrease caused by the modelling of the water vaporisation. However, the temperature profile still shows an influence, which is illustrated by the gradual increase in temperature. The heat balance over the layers becomes constant immediately as the water content of a layer starts to evaporate. This results in a constant temperature in time. A possible solution for this problem is described by [Saastamoinen, 1999b], who deduced a linear relation between the water content and the front propagation velocity from measurements. By obtaining the relation from experimental data, intra-particle effects are taken into account. However, correct kinetic parameters can reduce the incorrect temperature profile. The influence of the kinetics is discussed in paragraph 6.3, where the calculated mass decrease is compared to the measured one.

The influence of the airflow is not well modelled. No influence at all is found on the mass decrease, which is probably caused by the incorrect specific heat exchange surface used during calculation. Therefore, this specific heat exchange surface has to be determined.

The model has to be extended with the influence of the oxygen concentration. A similar approach as deduced by [Saastamoinen, 1999b] for the water content could be a possibility. Extension of the kinetic modelling with the oxygen concentration is not advisable, due to fact that the combustion conditions are difficult to define during measurements. Therefore, it is difficult to obtain accurate kinetic parameters from experimental data.

6.3 Theory versus experiment

A comparison between the measured conversion and calculated conversion of biomass at an airflow of 20 l/min is shown in figure 6-4.

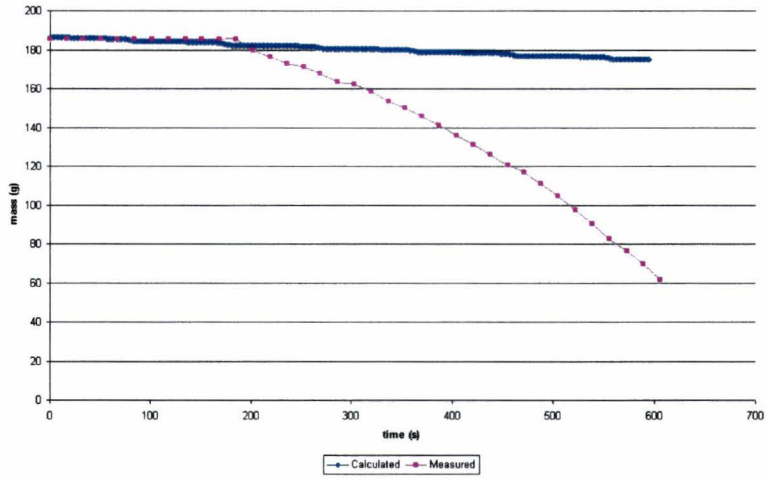

figure 6-4: ***Calculated mass decrease (200 layers, dt =0.001s) compared to the measured mass decrease at an airflow of 20 l/min and an inlet oxygen concentration of 21%***

A disparity in ignition time is found. The model describes an earlier conversion / ignition, probably caused by the assumption of an adiabatic process. Notable heat losses have occurred during measurements, which results in a slower ignition of the bed material.

Furthermore, the model differs from the measured data for the conversion rate / front propagation velocity. The modelled conversion rate is much slower than the real conversion rate of biomass into gas and tar. It is assumable that this difference is caused by incorrect kinetic parameters and by neglecting the conversion of char into gas and tar. This assumption is also confirmed by the lower maximum bed temperature described by the model, 515 K (figure 6-2) compared to the maximum temperature found during experiments, 800 K (figure 5-3). This in spite of the assumed adiabatic process, which should result in a higher maximum bed temperature. Beside that, it is probable that correct kinetics will improve the problems of the water vaporisation on the temperature profile.

7 Conclusion and recommendations

A clear influence is found for the airflow and oxygen concentration on the temperature. In turn, a relation is found between the temperature and the release of species from the bed. However, the deduced relation is only a trend instead of the amount released as function of temperature. This, due to the diversity of the data obtained with the different measurement techniques. The found trends of the oxygen concentration and airflow in relation to the temperature and total conversion of biomass are listed in Table 7-1.

Table 7-1: The influence of the airflow and the oxygen concentration on the temperature and the emission of species

Influence parameter	*Influence on the temperature*	*Influence on the emission of species*
An increase of the airflow results in	no influence on the ignition time	negligible influence on the start point of emission
	a higher reaction front propagation velocity	a shorter release of species
	a shorter combustion time	
	higher maximum bed temperature	a lower conversion
An increase of the oxygen concentration results in	an earlier ignition	an earlier release
	shorter combustion time	a shorter period at which emissions occur
	a higher reaction front propagation velocity	
	a higher maximum bed temperature	a higher conversion

A 1-D model is written to describe the emission of species during biomass fixed bed combustion. The bed is divided into layers, whereby over each layer the energy and mass balances are formulated, extended with a kinetic model formulating chemical reactions. At the moment, the model is not able to describe the temperature profile in the bed. Therefore, further research is necessary to calculate the temperature profile more accurate. An accurate description of the temperature profile in the bed would make it possible to extend the model with experimental obtained relations between the temperature and the emission of species.

The used kinetics are the main issue of inaccuracy. Improvement of these parameters can be done by a literature research or by investigating the conversion of wood into gas, tar and char experimentally. Taking into account the conversion of char into gas and tar could also lead to better results.

Further recommendations can be made on the modelling field and on the experimental field.

Concerning the model the following recommendations can be made:

- At the moment, the model shows an earlier ignition compared to the experimental results. Occurring heat losses, which are neglected in the model, probably cause this difference. Therefore, the influence of heat losses should be investigated.

- The influence of the water vaporisation on the conversion and temperature profile has to be investigated. A possible solution for taking into account the influence of the water content correctly is described by [Saastamoinen, 1999b], who deduced a linear relation between the water content and the front propagation velocity from measurements. Intra-particle effects are taken into account by obtaining the relation from experimental data.

- At the moment, no influence of the airflow is found on the release of species from the fuel bed. Therefore, the specific heat exchange surface has to be determined.

- The model has to be extended in order to take the influence of the oxygen concentration into consideration.

- The influence of some parameters should be investigated to verify the sensitivity on the temperature profile. These are the following parameters:
  - radiation. The fuel bed is heated by two surfaces uniform in temperature, which is incorrect.
  - geometrical parameter (pore diameter) in the effective heat conductivity
  - material properties of the biomass and char

If necessary, a suggestion for describing the effective heat conductivity more accurately is described by [Saastamoinen]. In his work a solution is presented to deduce a relation between the airflow and the geometrical parameters like the emissivity, pore diameter and ignition length. This relation is deduced by transferring the energy equation into a relation describing the front propagation inside the bed by introducing a moving co-ordinate

Concerning the experimental work the following recommendations can be made:

- Clarify the diversity in data of the emissions released from the fuel bed. This is necessary to make it possible to express the release of species as function of the temperature. This relation should make it possible to implement the release of individual species in a model, which is only describing the temperature profile in the bed. This makes it possible to model the bed temperature with a global mechanism similar to the mechanism used in this report.

- Deducing better kinetic parameters to describe the conversion of wood into gas, tar and char. In addition, the kinetic parameters for the conversion of char into gas and tar have to be deduced.

After performing the research described above it should be possible to deduce a relation describing the emission of species as function of the temperature. Furthermore, the model should be able to describe the temperature profile in the bed correctly. After implementation of the relation between the temperature profile and the release of species from the fuel bed, it is possible to predict the emissions accurately at different conditions over the range of airflows and oxygen concentration measured.

A last recommendation is to consider the work of [Gort, 1995], who did similar research. However, with a different approach, since a propagating reaction front is modelled in stead of the temperature.

Reference

[Bejan, 1993] Bejan A., *Heat transfer*, John Wiley & Sons, Inc., New York: 1993

[Beuken, 2000] Beuken R., *Grid reactor experiments on pyrolysis & gasification of biomass*, Eindhoven university of Technology, Eindhoven: June 2000

[Bilbao] Bilbao R., Mastral J.F., Ceamanos J., Aldea M.E., *Influence of different variables on the combustion behaviour of wood*, in: Biomass for Energy and Industry: pag. 1427-1430, University of Zaragoza (Spain)

[DiBlasi, 1993] DiBlasi C., *Analysis of convection and secondary reaction effects within porous solid fuels undergoing pyrolysis*, in: Combustion Science and Technology, Vol. 90, pp. 315-340, 1993

[Fleckl] Fleckl T.,Jäger H., Obernberger I., *Combustion diagnostics at a biomass-fired grate furnace using FT-IR absorption spectroscopy for hot gas measurements*, Institute of Chemical Engineering Fundamentals and Plant Engineering, Technical University of Graz, Austria.

[Fogler, 1999] Scott Fogler H., *Elements of chemical reaction engineering*, 3rd edition, Prentice-Hall PTR, New Jersey: 1999

[Gort, 1995] Gort R., Brouwers J.J.H., *Theoretical analysis of the propagation of a reaction front in packed beds*, Department of Mechanical Engineering, Twente University, The Netherlands

[Hill, 2000] Hill S.C., Douglas Smoot L., *Modelling of nitrogen oxides formation and destruction in combustion systems*, Progress in energy and combustion science, Vol. 26, pp. 417-458, 2000

[Geijn, 2000] Van de Geijn, R., *Influence parameters on the release of nitrogen species from a fuel bed for several biomass fuels, Literature review*, University of Technology Eindhoven, The Netherlands: May 2000

[Keller, 1994] Keller R., *Primärmassnahmen zur NO_x-Minderung bei der Holzverbrennung mit dem Schwerpunkt der Luftstufung*, Laboratorium für Energie systeme, ETH Zürich, Juris Druck+ Verlag Dietikon: 1994

[Kemenade, 1999] Van Kemenade E., *Procestechnische constructies II*, Eindhoven University of Technology, Eindhoven: January 1999

[Kreith, 1986] Kreith F., Bohn M.S., *Principles of heat transfer*, 4th edition, Harper and Row, Publishers, New York: 1986

[Lamers, 1997] Lamers A., *Fysische modellen en numerieke methoden bij stromingsproblemen*, Technische Universiteit Eindhoven nr.4623, Eindhoven: November 1997

[Lans] Van der Lans, R.P. et.al., *Modelling and experiments of straw combustion in a grate furnace*, Technical University of Denmark, Lyngby, Denmark

[Lans, 1998] Van der Lans R.P., *Straw combustion in grate furnaces*, Technical University of Denmark, Lyngby, Denmark: November 1998

[Lans, 1998b] Van der Lans, R.P., *Straw combustion in a grate furnace, Fixed-bed experiments*, Technical University of Denmark, Lyngby (Denmark): November 1998

[Martin, 1977] Martin H., *Low Peclet number particle-to-fluid heat and mass transfer in packed beds*, Chemical Engineering Science Vol. 33, pp. 913-919, 1977

[Noll, 1993] Noll B., *Numerische Strömungsmechanik*, Springer, Berlin Heidelberg: 1993

[Perry, 1997] Perry R.H., Green D.W., *Perry's Chemical Engineers' Handbook*, 7th edition, McGraw-Hill, New York: 1997

[Rindt, 1998] Rindt C., *Fysische meetmethode, Deel I*, University of Technology, Eindhoven, The Netherlands: November 1998

[Saastamoinen] Saastamoinen J.J., Horttanainen M., Sarkomaa P., *Ignition wave propagation and release of volatiles in beds of wood particles*, in: Combustion Science and Technology, VTT Energy, Jyväskylä, Finland

[Saastamoinen, 1999] Saastamoinen J.J., Taipale R., *NO_x formation in grate combustion of wood*, in: journal Environmental combustion technologies, VTT Energy, Jyväskylä, Finland: June 1999

[Saastamoinen, 1999b] Saastamoinen J. et. al., *Experiments with a pot furnace and a prototype horzontal stoker burner*, VTT Energy, Jyväskylä, Finland: June 1999b

[Schreel, 1998] Schreel, K.R.A.M., De Goey, L.P.H., *Fysische meetmethode, deel II: optica en optische meetmethoden*, University of Technology Eindhoven, The Netherlands: December 1998.

[Siegel, 1991] Siegel R., Howell J.R., Lohrengel J., *Wärmeübertragung durch Strahlung, Teil 2: Strahlungsaustausch zwischen Oberflächen und in Umhüllungen*, Springer-Verlag, Berlin Heidelberg: 1991

[Skreiberg, 1997] Skreiberg Ø., *Theoretical and experimental studies on emissions from wood combustion*, The Norwegian University of Science and Technology, Trondheim: November 1997

[Thurner, 1981] Thurner F., Mann U., *Kinetic investigation of wood pyrolysis*, Ind. Eng. Chem. Process Des. Dev. Vol. 20, pp. 482-488, 1981

[VDI, Gh1] VDI-Wärmeatlas, *Wärmeübergang Partikel-Fluid in durchströmten Haufwerken (Gh 1)*, 7. Auflage 1994

[VDI, Ka7] VDI-Wärmeatlas, *Strahlung technischer Oberflächen (Ka 7)*, 7. Auflage 1994

[VDI, Le 1] *VDI Wärmeatlas, Druckverlust bei der Strömung durch schüttungen* (Le 1), 7. Auflage 1994

[Wartha, 1998] Wartha C., *An experimental study on fuel-nitrogen conversion to NO and N_2O and on carbon conversion under fluidized bed conditions*, University of Technology, Vienna, Austria: January 1998

[Weissinger] Weissinger A., Fleckl T., Obernberger I., *Investigation on the release of nitrogen compounds from the fuel bed in grate furnaces*, Graz University of Technology, Graz, Austria

[Weissinger, 2001] Weissinger A., *Experimentelle Untersuchungen und reaktionskinetische Simulationen zur NOx-Reduktion durch Primärmaßnahmen bei Biomasse-Rostfeuerungen*, Dissertation an der Technischen Universität Graz, Austria: 2001

[Zhou, 1998] Zhou J., *Fuel-Bound Nitrogen Evolution During Biomass Gasification*, Academic Dissertation, University of Hawaii, USA: 1998

Appendix A

Details concerning the modelling

A.1 Radiational heat flux

A.2 The discretization process

A.3 Matlab©-file of the model

A.1 Radiational heat flux

As mentioned before the fuel bed is heated by radiation elements placed at the side and at the top of the furnace. These area's have a different temperature, which makes it necessary to calculate the net heat flux by radiation with the matrix inversion method. This method is presented below, based on [Kreith, 1986]. Furthermore, the view factors will be determined in this appendix.

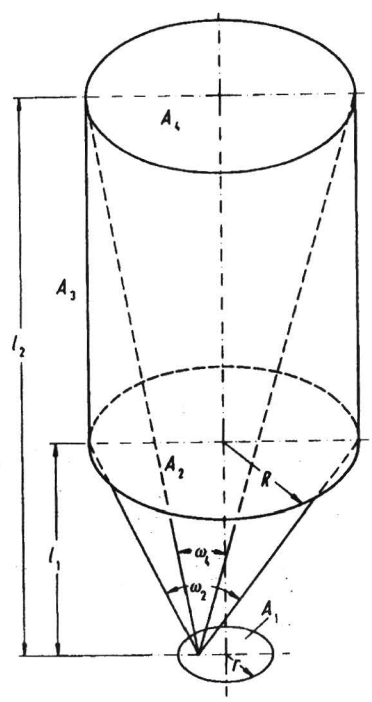

figure A-1: *Radiation exchange between the oven and the fuel bed surface [Siegel, 1991]*

The heat flux on a surface is the heat flux received minus the heat flux emitted, which is defined in the equation A-1.

$$(q_i)''_{net} = \frac{\varepsilon_i}{1-\varepsilon_i} \cdot (E_{bi} - J_i) \qquad \textit{(A-1)}$$

Whereby, ε is the emissivity of the surface and E_b is the emissive power. The radiosities, J of the surfaces are unknown. For the furnace, which is a grey enclosure consisting of three surfaces at specified temperatures, the different heat fluxes are defined in equation A-2.

$$(q_1)''_{net} = \frac{\varepsilon_1}{1-\varepsilon_1} \cdot (E_{b1} - J_1) = J_1 - J_1 F_{1-1} - J_2 F_{1-2} - J_3 F_{1-3}$$

$$(q_2)''_{net} = \frac{\varepsilon_2}{1-\varepsilon_2} \cdot (E_{b2} - J_2) = J_2 - J_1 F_{2-1} - J_2 F_{2-2} - J_3 F_{2-3} \qquad \textit{(A-2)}$$

$$(q_3)''_{net} = \frac{\varepsilon_3}{1-\varepsilon_3} \cdot (E_{b3} - J_3) = J_3 - J_1 F_{3-1} - J_2 F_{3-2} - J_3 F_{3-3}$$

Whereby, F is the view factor. These equations can be rewritten in the following matrix form:

$$AJ = C$$

where A is a 3×3 *matrix*

$$A = \begin{bmatrix} a_{11} & a_{12} & a_{13} \\ a_{21} & a_{22} & a_{23} \\ a_{31} & a_{32} & a_{33} \end{bmatrix}$$

and J and C are column matrices consisting of three elements each

$$J = \begin{bmatrix} J_1 \\ J_2 \\ J_3 \end{bmatrix} \qquad \text{and} \qquad C = \begin{bmatrix} \dfrac{\varepsilon_1}{1-\varepsilon_1} \cdot E_{b1} \\ \dfrac{\varepsilon_2}{1-\varepsilon_2} \cdot E_{b2} \\ \dfrac{\varepsilon_3}{1-\varepsilon_3} \cdot E_{b3} \end{bmatrix} = \begin{bmatrix} J_1 \\ J_2 \\ J_3 \end{bmatrix} \qquad \textit{(A-3)}$$

Whereby, the elements of matrix A are defined as follows:

$$a_{ii} = \left(1 - F_{ii} - \frac{\varepsilon_i}{1-\varepsilon_i}\right) \qquad \text{and} \qquad a_{ij} = -F_{i-j} \qquad \textit{(A-4)}$$

The emissive power, E_b of the surface is equal to the product of the Stefan-Boltzmann constant and the temperature raised by 4.

The view factors caused by radiation of the top and sidewall of the furnace can be calculated according to the method described below. The view factor of the upper layer is described in equation A-5 [Bejan, 1993], which is equal to the view factor of two parallel discs on the same centreline as shown in figure A-2.

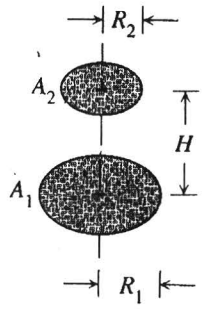

figure A-2 ***Two parallel discs on the same centreline [Bejan, 1993]***

$$F_{12} = \frac{1}{2}\left\{X - \left[X^2 - 4\left(\frac{x_2}{x_1}\right)^2\right]^{1/2}\right\} \qquad \textit{(A-5)}$$

where $x_1 = \dfrac{R_1}{H}$, $x_2 = \dfrac{R_2}{H}$ *and* $X = 1 + \dfrac{1 + x_2^2}{x_1^2}$

The view factor of the sidewall to the upper layer of the fuel bed can be calculated according to a method presented in [Siegel, 1991]. In figure A-1 the different areas are visualised. The view factor for an element dA_1 to the side of the furnace, A_3 is equal to the difference between the view factors from dA_1 to A_2 and A_4 [Siegel 1991]. Therefore, the view factor for the radiation from area A_1 to area A_3 is defined as follows:

$$F_{d1-3} = F_{d1-2} - F_{1-4} \qquad \textit{(A-6)}$$

After integration over the whole area A_1 and rewriting it for the view factor from the side of the furnace to the surface of the fuel bed, equation A-7 yields.

$$F_{3-1} = \frac{A_1}{A_3}\left(F_{1-2} - F_{1-4}\right) \qquad \textit{(A-7)}$$

The view factors from area A_4 and A_2 to the surface of the fuel bed can be described as two parallel discs on the same centreline as discussed before. After the view factors are known it is possible to calculate the radiosity of the fuel bed and therefore it is possible to calculate the net heat flux of the upper layer of the fuel bed.

A.2 Discretization process

[Lamers, 1997], [Noll, 1993]

In order to solve the energy equation for a layer in the bed as described in equation 3.5 the finite-difference method will be used. This method divides the fuel bed in control volumes, which are not overlapping each other. The temperature distribution in the furnace can be modelled one dimensional, because the horizontal gradient is negligible during grate combustion as discussed in chapter 2. The control volume, with the dimensions Δy*1*1, used for the discretization of the energy balance is illustrated in figure A-3.

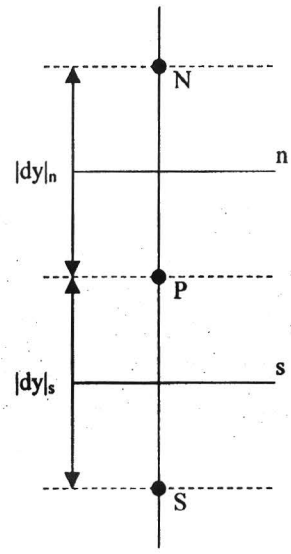

***figure A-3**: Control volume with the dimension Δy*1*1*

The finite-difference method calculates the function value in the middle of the control volume, point P and this value is considered to be valid over the entire control volume. So, the finite-difference method gives an approximation of the analytical solution. For the sake of completeness the energy equation of equation 3.5 is given below.

$$\rho \cdot c_p \cdot V \cdot \frac{\partial T}{\partial t} = k \cdot A \cdot \frac{\partial T}{\partial \bar{x}} + S \qquad \textit{(A-8)}$$
$$with: S = q_c + q_{vap} + q_{kin}$$

By integrating the separate terms of equation 3-8 over the control volume the 1-D differential equation occurs. Integration of the time-dependant term gives the following relation:

$$\rho \cdot c_p \int_s^n \int_t^{t+\Delta t} \frac{\partial T}{\partial t} dt dy = \rho \cdot c_p \cdot \left(\left. \frac{\partial T}{\partial t} \right|_{t+\Delta t} - \left. \frac{\partial T}{\partial t} \right|_t \right) \cdot \Delta y \qquad \textit{(A-9)}$$

Integration of the conduction term leads to the following equation, whereby the thermal conductivity, k is assumed to be constant over the time interval:

$$\int_s^n \int_t^{t+\Delta t} k \cdot \frac{\partial T}{\partial y}\, dtdy = \left(k \cdot \left.\frac{\partial T}{\partial y}\right|_n - k \cdot \left.\frac{\partial T}{\partial y}\right|_s \right) \cdot \Delta t \qquad \textit{(A-10)}$$

As discussed before in chapter 3 the heat flux caused by convection is supplemented in the source term, due to the fact that the area of heat transfer is different than the area of conductive heat transfer. Integration of the source term, last term in equation A-8, leads to equation A-11.

$$\int_s^n \int_t^{t+\Delta t} S\, dtdy = S_P \cdot \Delta t \cdot \Delta y \qquad \textit{(A-11)}$$

The source term, S_P of equation A-11 is the mean value of the source term over the control volume. It is possible to describe this term more accurately by linearisation of the source term. The source term is then divided in a part, which is constant, S_{P0} and a part, which is a function of the parameter Φ, S_Φ. This leads to the following equation.

$$\int_s^n \int_t^{t+\Delta t} S\, dtdy = \left(S_{P0} + S_\Phi \cdot \Phi\right) \cdot \Delta t \cdot \Delta y \qquad \textit{(A-12)}$$

Substitution of equation A-9 till equation A-12 into equation A-8 leads to the following 1-D differential equation for the energy balance over the control volume:

$$\rho \cdot c_p \cdot \left(\left.\frac{\partial T}{\partial t}\right|_{t+\Delta t} - \left.\frac{\partial T}{\partial t}\right|_t \right) \cdot \Delta y = \left(k \cdot \left.\frac{\partial T}{\partial y}\right|_n - k \cdot \left.\frac{\partial T}{\partial y}\right|_s \right) \cdot \Delta t + \left(S_{P0} + S_\Phi \cdot \Phi\right) \cdot \Delta t \cdot \Delta y \qquad \textit{(A-13)}$$

The subscripts in equation A-13 describe the place where the functions are counted out. The function values at the border of the control volume can be counted out by making use of the central differential scheme. This scheme is based on the Taylor's series expansion of a parameter in a point in the place and time, which is showed for the temperature in equation A-14 and equation A-15.

$$T(x+\Delta x,t) = T(x,t) + \frac{\partial T}{\partial x}(x,t) \cdot \Delta x + \frac{\partial^2 T}{\partial x^2}(x,t) \cdot \frac{\Delta x^2}{2!} + \frac{\partial^3 T}{\partial x^3}(x,t) \cdot \frac{\Delta x^3}{3!} + O\left(\Delta x^4\right) \qquad \textit{(A-14)}$$

$$T(x-\Delta x,t) = T(x,t) - \frac{\partial T}{\partial y}(x,t) \cdot \Delta x + \frac{\partial^2 T}{\partial x^2}(x,t) \cdot \frac{\Delta x^2}{2!} - \frac{\partial^3 T}{\partial x^3}(x,t) \cdot \frac{\Delta x^3}{3!} + O\left(\Delta x^4\right) \qquad \textit{(A-15)}$$

By adding equation A-14 up to equation A-15 and neglecting terms smaller than $O(\Delta x^2)$ the following expression is found for the temperature in point (x,t), according to the central differential scheme.

$$T(x,t) = \frac{1}{2} \cdot \left(T(x+\Delta x,t) + T(x-\Delta x,t)\right) + O(\Delta x) \qquad \textit{(A-16)}$$

By subtracting equation A-15 from equation A-14 and neglect terms smaller than $O(\Delta x^3)$ the following expression is found for the temperature gradient, according to the central differential scheme.

$$\frac{\partial T}{\partial x}(x,t) = \frac{\left(T(x+\Delta x,t) - T(x-\Delta x,t)\right)}{2 \cdot \Delta x} + O(\Delta x^2) \qquad \textit{(A-17)}$$

The temperature and the temperature gradient at the border of the control volume can now be expressed as a function of the values valid in the control volume. The conditions valid at the border in point n are then as follows:

$$T_n = \frac{1}{2} \cdot (T_N + T_P)$$

$$\left.\frac{\partial T}{\partial y}\right|_n = \frac{(T_N - T_P)}{\Delta y} \qquad \textit{(A-18)}$$

After substitution of equation A-18 into equation A-13 and rewriting the conditions at point s on the border of the control volume the following expression for the energy balance yields:

$$\frac{\rho \cdot c_p \cdot \Delta y}{\Delta t} \cdot \left(T_P - T_P^0\right) = k_n \cdot \frac{T_N - T_P}{\Delta y} - k_s \cdot \frac{T_P - T_S}{\Delta y} + \left(S_{P0} + S_\Phi \cdot \Phi\right) \cdot \Delta y \qquad \textit{(A-19)}$$

Whereby the upwind scheme is used for the differentiation of the time dependency. With T_P^0 defined as the temperature at t and T_P as the temperature at t+Δt. After rewriting equation A-19 by writing all the terms with T_P at the left side the following equation yields for the energy balance in a control volume:

$$a_P T_P = a_N T_N + a_S T_S + b$$

$$a_P = a_P^0 + a_N + a_S$$

$$a_N = \frac{k_n}{\Delta y}$$

$$a_S = \frac{k_s}{\Delta y} \qquad \textit{(A-20)}$$

$$b = a_P^0 T_P^0 + S\Delta y$$

$$a_P^0 = \frac{\rho \cdot c_p \cdot \Delta y}{\Delta t}$$

All the coefficients of equation A-20 have to be positive in order to get a stable equation. The following criteria can be derived out of the demand that $a_P > 0$:

$$a_P = \frac{\rho \cdot c_p \cdot \Delta y}{\Delta t} + \frac{2k}{\Delta y} > 0 \quad \rightarrow \quad \frac{\rho \cdot c_p \cdot \Delta y}{\Delta t} > -\frac{2k}{\Delta y} \quad \rightarrow \quad \frac{\alpha \cdot \Delta t}{\Delta y^2} < \frac{1}{2} \qquad \textit{(A-21)}$$

Where α is the thermal diffusivity ($=k/\rho c_p$). In order to derive the demand out of equation A-21 the thermal conductivity coefficients, k_n and k_s are taken equal. The limitation of the time interval, Δt and the place interval, Δx is defined by equation A-21 in order to keep a stable solution.

A.3 Matlab©-file of the model

As mentioned before the model is written in Matlab©. In order to reduce the calculation time it is chosen to write the model in a less suitable way. This method divides the layers of the bed into parts, which have the same condition: heating up, vaporisation or combusting. After the layers at which a certain condition is valid all the layers are calculated immediately instead of 'walking' through the bed and define the conditions constantly for each layer. This way of modeling reduced the calculation time with a factor 10. At the moment calculation takes about 48 hours to simulate 30 minutes real combustion time (200 layers, dt =0.001s). In this appendix the model is presented with additional remarks to clarify the model. The used functions are self-explaining and therefore not included. On request the model is available on disc including all the functions. The model is also available on the more "common way" of modeling. However, this model is not totally updated to the changes made during modeling.

MAIN PROGRAM

Definition of the used constants:

```
clear all

airflow    =  20;                  % airflow [l/min]

% input of the time and place step in order to satisfy the following
% demands:
%   apo   >  0
%   an    >  0
%   as    >  0
%   ap    >  0

dt         = 0.001;                   % timesteps [s]
Nel        = 200;                  % Number of slices

X          = 1;                    % conversion
T          = [];
Temp       = [];
afst       = [];
ma         = [];
mass       = [];

% data of the fuel bed
height     = 10e-2;                % height of the furnace [m]
d          = 9.5e-2;               % diameter of the fuel bed [m]
A          = 0.25*pi*d*d;          % Surface of the fuel bed [m2]
V          = A*height;             % Volume of the fuel bed [m3]
Tstart     = 293;                  % Temperature of the fuel bed at t=0 [K]
dy         = height/Nel;           % height of the slices [m]
l          = 181e-3;               % distance between the top and the fuel bed

% data of the biomass material
M          = 0.185;                % Mass of the biomass
mli        = M/Nel;                % Initial mass of each layer [kg]
fvi        = 0.09;                 % Moisture content initially present in the
           particle
mld        = (1-fvi)*mli;          % Mass of each layer after complete
           evaporation [kg]
cp         = 2.3E3;                % heat capacity of the biomass material
```

```
dp          = 8.6137e-3;            % mean diameter of particles [m]
kb          = 10.46E-2;             % thermal conductivity of the biomass
kc          = 10.46E-2;             % thermal conductivity of the char [W/mK]

% calculating the porosity of the fuel bed
rho         = 643;                  % density of the biomass material [kg/m3]
Vf          = M/(rho);              % the volume of all the particles
together[m3]
psi         = (V-Vf)/V;             % the void fraction [-]

% calculating the convective heat exchange surface per layer based on the
% assumption of a bed filled with spherical particles
av          = (((Vf/Nel)/((4/3)*pi*(dp/2)*(dp/2)*(dp/2)))*pi*dp*dp)/(Vf/Nel)

% data of the airflow entering the fuel bed
m           = (airflow*1e-3)/60;       % Inlet airflow [m3/s]
ug          = m/A;                  % calculation of the airflow rate of fluid
per unit sectional area, whereby the cross section is empty
cpg         = 1.093e3;                 % specific heat of air [J/kgK]
alpha       = 1.14e-4;                 % thermal diffusivity of air taken at
500C
kg          = 25.77e-3;             % thermal conductivity of the air [W/mK]
Pr          = 0.7;

sigma = 5.67e-8;                    % Stefan Boltzman constant [W/m2K4]
```

During calculation the matrix is build up as visualized below.

$$\begin{bmatrix} t & layer1\ layer2 --- the\ upper\ layer \\ t+dt & layer1\ layer2 --- the\ upper\ layer \end{bmatrix}$$

The first row consisting of the condition in every layer at t and the second row consisting of the conditions, which have to be calculated for t= t + dt. During the calculations the mass and the temperature are stored in the matrix. Therefore, the starting conditions are defined below:

```
afst(1,1) =  height-0.5*height/Nel;
for i=2:Nel
   afst(i,1) =  afst(i-1,1)-height/Nel;
end

T(1,1)           = 0;               % Matrix building whereby the first column
is the time
ma(1,1)          = 0;               % Matrix building whereby the first column
is the time
T(1,2:Nel+1)  = Tstart;
ma(1,2:Nel+1) = mli;
Tg(1,1:Nel)      = 293;             % Temperature of the gas stream entering
the furnace
%%%%%%%%%%%%%%%%%%%%%%%%%%%%%%%%%

z   = Nel/100;
j   = 1;

for i=1:Nel
   if z   < (Nel/100)
      z   = z + 1;
   else
      j   = j + 1;
   Temp(1,1) = 0;
   Temp (1,j)   = Tstart;
      mass(1,1) = 0;
   mass(1,j)     = mli;
   z = 1;
  end
end
```

```
y   = 999;
wtjes = 9;

while T(1,1)<1800    % Time limitation of 30 min combustion time

z = (Nel/100);
j = 1;
```

The data is written automatically to a text-file in order to limit the size of the matrix. This made it possible to calculate with only two timesteps as shown before.

```
if y<999
   y=y+1;
   else
   % save temperature data  in text file 'berekeningT'
   fid    =   fopen('berekeningTimpl200.txt','a');
      fprintf(fid,'%6.1f %12.2f %18.2f %24.2f %30.2f %36.2f %42.2f %48.2f
%54.2f %60.2f %66.2f %72.2f %78.2f %84.2f %90.2f %96.2f %102.2f %108.2f
%114.2f %120.2f %126.2f %132.2f %138.2f %144.2f %150.2f %156.2f %162.2f
%168.2f %174.2f %180.2f %186.2f %192.2f %198.2f %204.2f %210.2f %216.2f
%222.2f %228.2f %234.2f %240.2f %246.2f %252.2f %258.2f %264.2f %270.2f
%276.2f %282.2f %288.2f %294.2f %300.2f %306.2f %312.2f %318.2f %324.2f
%330.2f %336.2f %342.2f %348.2f %354.2f %360.2f %366.2f %372.2f %378.2f
%384.2f %390.2f %396.2f %402.2f %408.2f %414.2f %420.2f %426.2f %432.2f
%438.2f %444.2f %450.2f %456.2f %462.2f %468.2f %474.2f %480.2f %486.2f
%492.2f %498.2f %504.2f %510.2f %516.2f %522.2f %528.2f %534.2f %540.2f
%546.2f %552.2f %558.2f %564.2f %570.2f %576.2f %582.2f %588.2f %594.2f
%600.2f %606.2f\n', Temp(1,:));   % save mass data in text file
'berekeningm'
   fit2   =   fopen('berekeningmimpl200.txt','a');
   fprintf(fit2,'%6.1f %12.5f %18.5f %24.5f %30.5f %36.5f %42.5f %48.5f
%54.5f %60.5f %66.5f %72.5f %78.5f %84.5f %90.5f %96.5f %102.5f %108.5f
%114.5f %120.5f %126.5f %132.5f %138.5f %144.5f %150.5f %156.5f %162.5f
%168.5f %174.5f %180.5f %186.5f %192.5f %198.5f %204.5f %210.5f %216.5f
%222.5f %228.5f %234.5f %240.5f %246.5f %252.5f %258.5f %264.5f %270.5f
%276.5f %282.5f %288.5f %294.5f %300.5f %306.5f %312.5f %318.4f %325.5f
%330.5f %336.5f %342.5f %348.5f %354.5f %360.5f %366.5f %372.5f %378.5f
%384.5f %390.5f %396.5f %402.5f %408.5f %414.5f %420.5f %426.5f %432.5f
%438.5f %444.5f %450.5f %456.5f %462.5f %468.5f %474.5f %480.5f %486.5f
%492.5f %498.5f %504.5f %510.5f %516.5f %522.5f %528.5f %534.5f %540.5f
%546.5f %552.5f %558.5f %564.5f %570.5f %576.5f %582.5f %588.5f %594.5f
%600.5f %606.5f\n', mass(1,:));
      fclose('all');
      y   = 0;
   end

   T(2,1)     = T(1,1) + dt;          % calculating the time
   Temp(2,1)  = Temp(1,1) + dt;
   ma(2,1)       = ma(1,1) + dt;         % calculating the time
   mass(2,1)  = mass(1,1) + dt;

   %for i=1:Nel
      % definition of the temperatures in the bed
      Tpo(1,1:Nel)   = T(1,2:Nel+1);

      Ts(1,1:Nel-1) = T(1,3:Nel+1);
      Ts(1,Nel)      = T(1,Nel+1);

      Tn(1,1)        = 293;
      Tn(1,2:Nel)       = T(1,2:Nel);

      % calculation of the thermal conductivity [W/mK]
      k          =   kmean2(X, Tpo, dp, kb, kc, kg, sigma);

      % calculation of the discretization parameters
      apo(1,1:Nel) = (rho*cp*dy)/dt;
```

```
%if apo<=0
%   warning('error in apo')
%end

as = k./dy;
%if as<=0
%   warning('error in as')
%end

an = k./dy;
%if an<=0
%   warning('error in an')
%end

ap = apo + as + an;
%if ap<0
%   warning('error in ap')
%end
```

Separate the different zones over the bed, by walking through the first layer and check at which condition a layer is at t

```
p  = 0;
w  = 1;
w1 = 0;
w2 = 0;
w3 = 0;

while p < Nel
 p = p + 1;

   if T(1,p+1) < 373          % determining the pre-heat zone
      w  = w + 1;
    end

    if ma(1,p+1) > mld        % determining the vaporisation zone
       w1  = p + 1;
    end

    if ma(1,p+1) > 1e-10      % determining the combustion zone
       w2 = p + 1;
    end

     if ma(1,p+1) < 1e-10       % determining the upper layer
     w3 = p;
        p  = Nel+1;
     end
end

if ma(1,Nel+1) > 1e-10
   w3 = Nel + 1;
end

if w == w3
   w = w-1;
end

if w1 == w3
   w1 = w1-1;
end

if w2 == w3
   w2 = w2-1;
end

if w2 == w1
```

```
    w2 = 0;
end

if w1 == w
    w1 = 0;
end
```

The actual calculation of the temperature and mass in the bed, making use of the model described in chapter 3

```
% heating up till 373 K.
S                 = qc2(Tpo,Tg,ug,k,psi,dp,(w-1));
T(2,2:w)          = (apo(1,1:w-1).*Tpo(1,1:w-1)+ an(1,1:w-1).*Tn(1,1:w-1) +
                  as(1,1:w-1).*Ts(1,1:w-1) - S(1,1:w-1))./ap(1,1:w-1);
ma(2,2:w)         = ma(1,2:w);

if w1 > 0
   if w1 > w
     % vaporisation of the water.
   % Assumption: water vaporisation temperature is 473 K. The temperature
      % of the layer will be constant and the energy storage in time is
zero.
      % Therefore the energy equation becomes:
      hfg           = Mois2(T(1,w+1:w1));
      main          = ma(1,w+1:w1);
      maout         = main / (1-((dt/rho).*(an(1,w:w1-1).*(Tpo(1,w:w1-1)-
                  Tn(1,w:w1-1)) + as(1,w:w1-1).*(Tpo(1,w:w1-1)-Ts(1,w:w1-1)) -
                  qc2(Tpo(1,w:w1-1),Tg(1,w:w1-1),ug,k(1,w:w1-1),psi,dp,(w1-
                  w))))./(hfg(1,1:w1-w).*dy));
      ma(2,w+1:w1)  = maout;
      T(2,w+1:w1)   = T(1,w+1:w1);
   else
       hfg              = Mois2(T(1,w1));
      main          = ma(1,w1);
      maout         = main / (1-((dt/rho).*(an(1,w1-1).*(Tpo(1,w1-1)-
                  Tn(1,w1-1)) + as(1,w1-1).*(Tpo(1,w1-1)-Ts(1,w1-1)) -
                  qc2(Tpo(1,w1-1),Tg(1,w1-1),ug,k(1,w1-
                  1),psi,dp,1))).*(hfg(1,1).*dy));
      ma(2,w1)      = maout;
      T(2,w1)       = T(1,w1);
   end
end

if w2 > 0
   % heating up and occuring reactions in the bed
   if w1 > 0
      MAIN          = ma(1,w1+1:w2);
      Cwold         = ma(1,w1+1:w2)./(V/Nel);  % Concentration WOOD in the
layer

      S             = qc2(Tpo(1,w1:w2-1),Tg(1,w1:w2-1),ug,k(1,w1:w2-
                    1),psi,dp,(w2-w1)) + qkin2(Tpo(1,w1:w2-1), psi, Cwold,
                    0).*dy;
      T(2,w1+1:w2)  = (apo(1,w1:w2-1)*Tpo(1,w1:w2-1) + an(1,w1:w2-
                    1)*Tn(1,w1:w2-1) + as(1,w1:w2-1)*Ts(1,w1:w2-1) -
                    S(1,1:w2-w1))/ap(1,w1:w2-1);
   % Suppress the bed temperature to extrem values
      if T(2,w1+1:w2) > 1500
         T(2,w1+1:w2) = 1500;
      end
      Cwnew         = Cwood2(Tpo(1,w1:w2-1), Cwold(1,1:w2-w1), dt);
      maout         = Cwnew.*(V/Nel);
      ma(2,w1+1:w2) = maout;
   else
      MAIN          = ma(1,w2);
      Cwold         = ma(1,w2)./(V/Nel);    % Concentration WOOD in the layer
```

```
      S              = qc2(Tpo(1,w2-1),Tg(1,w2-1),ug,k(1,w2-1),psi,dp,1) +
                     qkin2(Tpo(1,w2-1), psi, Cwold, 0).*dy;
      T(2,w2)        = (apo(1,w2-1)*Tpo(1,w2-1) + an(1,w2-1)*Tn(1,w2-1) +
                     as(1,w2-1)*Ts(1,w2-1) - S(1,1))/ap(1,w2-1);
      if T(2,w2) > 1500
         T(2,w2) = 1500;
      end
      Cwnew          = Cwood2(Tpo(1,w2-1), Cwold(1,1), dt);
      maout          = Cwnew.*(V/Nel);
      ma(2,w2)       = maout;
   end
end

% UPPER LAYER OF THE BED:
if w3 > 0
   if T(1,w3) < 373
      l              = 181e-3 + (Nel+1-w3)*dy;
      S1             = qc(Tpo(1,w3-1),Tg(1,w3-1),ug,k(1,w3-1),psi,dp) +
                        radiation(Tpo(1,w3-1), sigma, l);
     Tnew            = (apo(1,w3-1)*Tpo(1,w3-1) + an(1,w3-1)*Tn(1,w3-1) -
                        S1)/(apo(1,w3-1) + an(1,w3-1));
      ma(2,w3)       = ma(1,w3);
      T(2,w3)        = Tnew;
    else
      if ma(1,w3) > mld
         l              = 181e-3 + (Nel+1-w3)*dy;
         hfg            = Mois2(Tpo(1,w3-1));
         main           = ma(1,w3);
          ma(2,w3)      = main / (1-((dt/rho)*(radiation(Tpo(1,w3-2), sigma,
                        l) - an(1,w3-1)*(Tpo(1,w3-1)-Tn(1,w3-1)) -
                        qc(Tpo(1,w3-1),Tg(1,w3-1),ug,k(1,w3-
                        1),psi,dp)))/(hfg*dy));
          T(2,w3)       = T(1,w3);
      else
         if ma(1,w3) < 1e-10
            ma(2,w3:Nel+1) = 0;
            T(2,w3:Nel+1)  = T(1,w3-1:Nel); %!!!!!!!!!!!!!!!1
         else
            l           = 181e-3 + (Nel+1-w3)*dy;
            main        = ma(1,w3);
            Cwold       = main/(V/Nel);
            S2          = radiation(Tpo(1,w3-2), sigma, l) + qc(Tpo(1,w3-
                     1),Tg(1,w3-1),ug,k(1,w3-1),psi,dp) + qkin(Tpo(1,w3-1),
                     psi, Cwold, 0)*dy;
            T(2,w3)     = (apo(1,w3-1)*Tpo(1,w3-1) + an(1,w3-1)*Tn(1,w3-1) -
                     S2)/(apo(1,w3-1) + an(1,w3-1));
            if T(2,w3) > 1500
               T(2,w3) = 1500;
            end
            Cwnew       = Cwood(Tpo(1,w3-1), Cwold, dt);
            ma(2,w3)    = Cwnew*(V/Nel);
         end
      end
   end
end
```

Reducing the matrix for calculation into a matrix consisting of 101 columns, which is used to save the data in the before mentioned text file

```
for i=1:Nel
   if z < (Nel/100)
       z = z + 1;
   else
       j              = j + 1;
       T2             = T(2,i+1);
       ma2            = ma(2,i+1);
```

```
        Temp (2,j)    = T2;
        mass(2,j)        = ma2;
        z             = 1;
    end
end

% Calculating the gas temperature leaving the layer
Re         = (RhoFl2(Tg(1,1:Nel), Nel).*(ug*dp))./(Mug2(Tg(1,1:Nel),
Nel).*psi);
Nu         = Nusselt2(Re(1,1:Nel),Pr,psi);
Pe         = Re(1,1:Nel).*Pr;
NTU    = (Nu(1,1:Nel).*(av*height))./Pe(1,1:Nel);

for i = 1:Nel
    if i > 1
        Tgas       = Tg(1,i-1);
        Tg(2,i)    = (Tgas-Tpo(1,i))*exp(-1*NTU(1,i)) + Tpo(1,i);
    else
        Tg(2,i)    = (293-Tpo(1,i)).*exp(-1*NTU(1,i)) + Tpo(1,i);
    end
end
```

Overwrite the first row consisting the old data with the new data of the second row

```
T(1,:)     = T(2,:);
Temp(1,:)  = Temp(2,:);
ma(1,:)    = ma(2,:);
mass(1,:)  = mass(2,:);
Tg(1,:)    = Tg(2,:);
end
```

Appendix B

Experimental details

B.1 Experimental plan

The experimental plan is described in this appendix. First of all some general procedures will be outlined followed by the specific experimental plan for the airflow and oxygen concentration. The chapter ends with a schematic overview of all the measurements performed.

The reproducibility of the measurements is checked, by repeating all measurements three times. The average value is used to find the tendency of a certain parameter.

Definitions:

- The measurements are started at the moment that the radiation elements on the side and the top of the furnace reach a temperature of respectively 450 and 750°C.
- The radiation elements are heating the bed constantly during the test run.
- The measurement is stopped at the moment that the temperature of the lowest thermocouple in the fuel bed has decreased till 700°C. This means that most of the char combustion has taken place.
- Some measurements are performed with an external FT-IR present. This is listed in the overview presented in chapter B.1.3.
- The bottles for the wet analyse method are filled according to the following solution:

  1 bottle: 100 ml 0.1 M H_2SO_4
  2 bottles: 96.7 ml 0.1 M NaOH + 3.3 ml 0.117 M $Pb(CH_3COO)_2$

B.1.1 Airflow

Changing the airflow rate will lead to a change in the combustion time and to a change in the bed temperature. The influence of those on the release of species is not clear from literature and has to be investigated.

In order to find the influence of the airflow the following experiment is performed:
The following conditions are prepared:

- The fuel-type and the weight of the fuel bed will be chosen constant at 180 grams, which corresponds to a full bed. The particle size is between 5 and 20 mm with an experimental specified distribution in size.
- The oxygen concentration in the airflow is 20%, whereby the rest consists of molecular nitrogen.

Cooling of the Saphire-windows is done with a constant nitrogen flow of 3 l/min. The temperature, the mass of the fuel bed, the concentration of the nitrogen species (NO, NO_2, and NH_3) and the concentration of C_xH_y, CO, CO_2 and H_2O as function of time are measured during the test runs. The airflows investigated are 20, 25, 30, 35, and 40 l/min.

Number of airflow's measured:	5	***Number of experiments:***	15
Repetitions:	3	***Duration of the experiment:***	5 days

B.1.2 Oxygen concentration

In literature the influence of the oxygen concentration in the primary airflow is not clear during char combustion. However, it is not possible to investigate this influence separately from the gasification. Therefore, the general effect has to be found. According to the literature the general effect of an increase of the oxygen concentration leads to a higher conversion of fuel to NO_x. The explanation for this effect can be found in the influence of NH_i, which role changes for different conditions. Under oxidizing conditions is the conversion of NH_i to NO dominant and under reduced conditions is the conversion of NH_i to N_2 dominant. The exact role of NH_i on the production of NO has to be investigated.

In order to find the influence of NH_i on the production of NO the following experiment is performed:

- The fuel-type and the weight of the fuel bed is chosen constant at 180 grams.
- The airflow is taken constant at 30 l/min
- Cooling of the Saphire-windows is done at a constant flow of nitrogen.

The temperature, the mass of the fuel bed, the concentration of the nitrogen species (NO, NO_2, and NH_3) and the concentration of CO, CO_2, C_xH_y and H_2O as function of time are measured for the oxygen concentrations. The oxygen concentrations will be taken at 8, 12, 16, and 20 %. The oxygen concentration of 20 % is already measured during the airflow investigation. The desired oxygen concentration is obtained by mixing air with nitrogen. Before the airflow enters the fuel bed the oxygen concentration is measured as shown in figure 4.2. However, his method leads to inaccuracies in the flow rate.

Number of oxygen concentrations measured:	4
Repetitions:	3
Number of experiments:	9
Duration of the experiment:	3 days

B.1.3 Overview of the measurements performed

The experiments performed are listed in table B-1 and B-2 concerning the influence of the airflow and oxygen concentration respectively. Beside that some remarks are listed concerning the presents of Saphire windows, an external FT-IR and if there appeared some problems during the test run.

Table B-1: Overview and remarks concerning the experiments performed to investigate the influence of the inlet airflow

Experiment	*Airflow rate (l/min)*	*Saphire windows*	*Pressure over the diluter*	*Remarks*
1	30	No	No	-
2	35	No	No	-
3	30	No	No	-
4	20	No	No	Balance did not work
5	40	No	No	Heating belt was not on temperature
6	25	No	Yes	Pressure measurement didn't work; no NO peak diluter started to late
7	20	No	Yes	no NO peak
8	40	No	Yes	Pressure over the diluter is ~ 2000 Pa; no NO peak
9	30	no	Yes	Pressure over the diluter is ~ 2600 Pa; no NO peak
10	25	no	Yes	Filter is clean; Thermocouple 3 and 4 are mixed up
11	35	no	Yes	-
12	40	yes	Yes	-
13	35	yes	Yes	-
14	20	yes	Yes	-
15	25	yes	Yes	-
16	30	no	other diluter	External FT-IR, NOx-equipment didn't work, *Time difference between FT-IR and labview*
17	40	no	other diluter	External FT-IR, idem time Range changed 100 ppm
18	20	no	other diluter	External FT-IR, idem time Range changed 100 ppm
19	25	no	other diluter	External FT-IR, idem time Range changed 100 ppm

Table B-2: **Overview and remarks concerning the experiments performed to investigate the influence of the oxygen concentration**

Experiment	*Oxygen conc. (%)*	*Saphire windows*	*Pressure over the diluter*	*Remarks*
1	8	no	other diluter	External FT-IR O2 isn't measured
2	16	no	other diluter	External FT-IR
3	13	no	other diluter	External FT-IR
4	8	no	yes	Balance for 10 min
5	16	no	yes	O2 has to be multiplied with 21/22
6	13	no	yes	O2 has to be multiplied with 21/22 till 12:50:00
7	16	yes	yes	Diluter problems
8	12	yes	yes	Thermocouple 1 didn't work Dilutor problems
9	8	yes	yes	range changed often
10	13	no	yes	Thermocouple 1 didn't work
11	16	no	yes	Time difference between Labview and Balread

B.2 Measurement equipment

Background information of the measurement equipment used is listed in this appendix. The placement of the equipment is illustrated in figure 4.2.

B.2.1 Airflow meters

B.2.1.1 MGV-25 O_2/N_2 0-100% LN Industries

DISPLAYS CONCENTRATIONS %	MEASURES OF CONCENTRATIONS AT : Q=0.2K	Q=0.5K	
Constant outflow			
0	0.2	1.1	
20	18.1	19.8	
50	49.1	50.3	
80	80.7	80.5	
100	99.9	99.9	
Constant concentration			
30	29.3	30.9	
60	60.2	60.5	

Outflow l/min	DISPLAY	MEASURED	
60% of O2	**0 K**	< 20 cc/min	
	0.1 K	0.7	l/min
	0.5 K	10.3	
	1 K	18.2	

B.2.1.2 RS Components AWM 5104

SPECIFICATIONS

Recommended power supply (1)		10 ± .01 VDC
Minimum power supply		8.0 VDC
Maximum power supply		15.0 VDC
Power consumption		100 mW max.
Output type		Linear, 1 to 5 VDC
Calibration gas	Suffix	VA = Argon VC = CO_2 Carbon Dioxide, N_2O Nitrous Oxide VN = N_2 Nitrogen, O_2 Oxygen, Air
Gas flow range	AWM5101	0 to 5 SLM (5)
	AWM5102	0 to 10 SLM
	AWM5103	0 to 15 SLM
	AWM5104	0 to 20 SLM
Output at laser trim point		5.0 VDC at Full Scale Flow
Differential pressure at full scale		See Pressure vs Flow Chart
Null output		1.00 ± 0.05 VDC
Null output shift, -20 to 70°C		± .050 VDC typ., ± .200 VDC max.
Full scale output shift, -20 to +25°C and +25 to +70°C (4)		Suffix VA or VN: ± 7.0 % F.S.O. Suffix VC: ± 10.0 % F.S.O.
Linearity error (2)		± 3.0% reading
Repeatability & hysteresis		± 0.5% Reading
Response time		60.0 msec max.
Temperature range, operating and storage		-20 to +70°C (-4 to +158°F)
Termination (0.100" centers)		0.025" square
Connector (4 pin receptacle), included (3)		AMP (103956-3)
Weight		60 grams (2.06 oz.)
Shock rating		100 g peak, 6 msec half-sine (3 drops, each direction of 3 axes)
Vibration rating		15 g, 10-2000-10 Hz
Overpressure		50 psi max.
Leak rate, max.		0.1 psi/min. at static condition

1. Cannot guarantee calibration at supply voltages other than 10.0 ± 0.01 VDC.
2. Linearity specification applies from 2 to 100% full scale of gas flow range and does not apply to null output at 0 SLM.
3. Supplied in strip form. Other strip form receptacles are available as are various tools to assemble receptacles in strip form. Individual receptacle assemblies are also available from Amp.
4. SLM sensors have larger Full scale shifts over temperature. 0-20 SLM sensors have lowest shifts with respect to temperature.
5. SLM denotes standard liters per minute which is a flow measurement referenced to standard conditions of 0°C, 760 torr (sea level), 50% RH.

B.2.2 Gas Analysers

B.2.2.1 Eco Physics CLD 700 EL ht

2.1 Leistungskenndaten

Leistungskenndaten des CLD 700 EL ht

Messbereiche	0 – 10			
	0 – 100			
	0 – 1'000			
	0 – 10'000			
Signal-Rauschen, 1 σ	0,5% des Messbereichsendwert			
Min. Nachweisgrenze [ppm]:	0,1[2)]			
Querempfindlichkeit:				
Wasserdampf:	< 0,5% pro Vol % H_2O			
Kohlendioxid:	< 0,1% pro Vol % CO_2			
Nullpunktdrift:	keine			
Messbereich [ppm]:	10'000	1'000	100	10
Totzeit [sec]:[2)]	4	4	5	5
Anstiegszeit [sec] (0 – 90%):[2)]	4	4	8	16
Abfallzeit [sec] (0 – 90%):[2)]	4	4	8	16
Linearität: (im Bereich)	+/- 1% Vollausschlag			

[2)] Filter-Einstellung: standard

B.2.2.2 Fisher-Rosemount MLT-1/2-19" Analyser

Hersteller	Rosemount
Typ	NGA 2000
Meßbereich	0 - 5 % bis 0 - 100 % O_2
Ansprechzeit	≤ 5 sec
Linearität	≤ 1 %
Nullpunktdrift	≤ ± 1,0 % pro Woche
Empfindlichkeitsdrift	≤ ± 2 % pro Woche
Werkstoffe der gasführenden Teile	Edelstahl, PTFE
Meßgasmenge	ca. 1 l/min
Meßwertausgang	4 - 20 mA (analog)
Eingesetzter Meßbereich	0 – 21,5 %
Probengasentnahmesonde	Edelstahlrohr
Probengasfilter	beheiztes Keramikfilterelement
Probengasleitung	beheizter Teflonschlauch
Nullgas	Stickstoff 5.0
Kalibriergas	10,08 Vol.-% O_2
Genauigkeit der Messung	
Untere Nachweisgrenze	≤ 1% O_2

B.2.2.3 Ansyco FT-IR Gas-Anlysator Gasmet Dx-4000

Allgemeine Parameter und Spektrometer

Meßprinzip:	Fourier Transform Infrarot, FT-IR
Interferometer:	Karussell- Interferometer (zuverlässig, wartungsfrei, unempfindlich auch gegen starke Stöße und Vibrationen)
Auflösung:	empfohlen für Gasgemische : 8 cm^{-1} (max. 4 cm^{-1})
Scan Frequenz:	10 Spektren / s
Optisches Material:	BaF_2
IR-Quelle:	SiC, 1550 K (5 Jahre Lebensdauer)
Wellenlängenbereich:	900 - 4 250 cm^{-1}
Netzversorgung:	110-250 V/ 50-60 Hz **und** 12 V DC
externer Notebook-PC	nicht enthalten, Anschluss über RS232, incl. Software für Windows 95/98/NT/2000
Option DTGS-Detektor	DTGS-Detektor für Messungen im erweiterten Wellenlängenbereich von 650 - 4250 cm^{-1}. Die optischen Materialien bestehen dann aus ZnSe. Es wird kein flüssiger Stickstoff für den Normalbetrieb von MCT und DTGS benötigt. N_2 fl. wird nur in besonderen Fällen verwendet, wo wesentlich mehr Schnelligkeit und Empfindlichkeit benötigt werden (Modell Cr2000i).

Optionen für stationäre Analysatoren Dx-PRO mit PC:
Analogausgänge und Analogeingänge, Alarmrelais

Gasmessungen

Meßkomponenten:	simultane Analyse von max. 30 IR-aktiven Komponenten anorganische Gase: CO_2, CO, NO, NO_2, N_2O, NH_3, SO_2, HCl, HF, HCN, CH_4, COS, CS_2, H_2O, SF_6, organische Komponenten: Alkane, Alkene, Aromaten, Aldehyde, Alkohole, Ketone, Ester, CKW, FCKW, Lösemittel, uva.
Applikationen:	Messung heißer Gase (Emission, Pyrolyse, Katalyse, Prozess) Raumluft (MAK), Abluft, Qualitätskontrolle, Forschung, Labor
Probennahme (Option):	Gaspumpe, Partikelfilter für Proben bei Normalbedingungen, heiße Probennahmesysteme (SYCOS P-HOT), Verdünnungssonde (SYCOS P-797), Stationäre Prozess- und Mehrpunkt-Messanlagen SYCOS mit Dx-PRO

B.3 Results of the measurements

The release of species as function of the airflow and oxygen concentration is illustrated in figure B-1 and B-2 respectively.

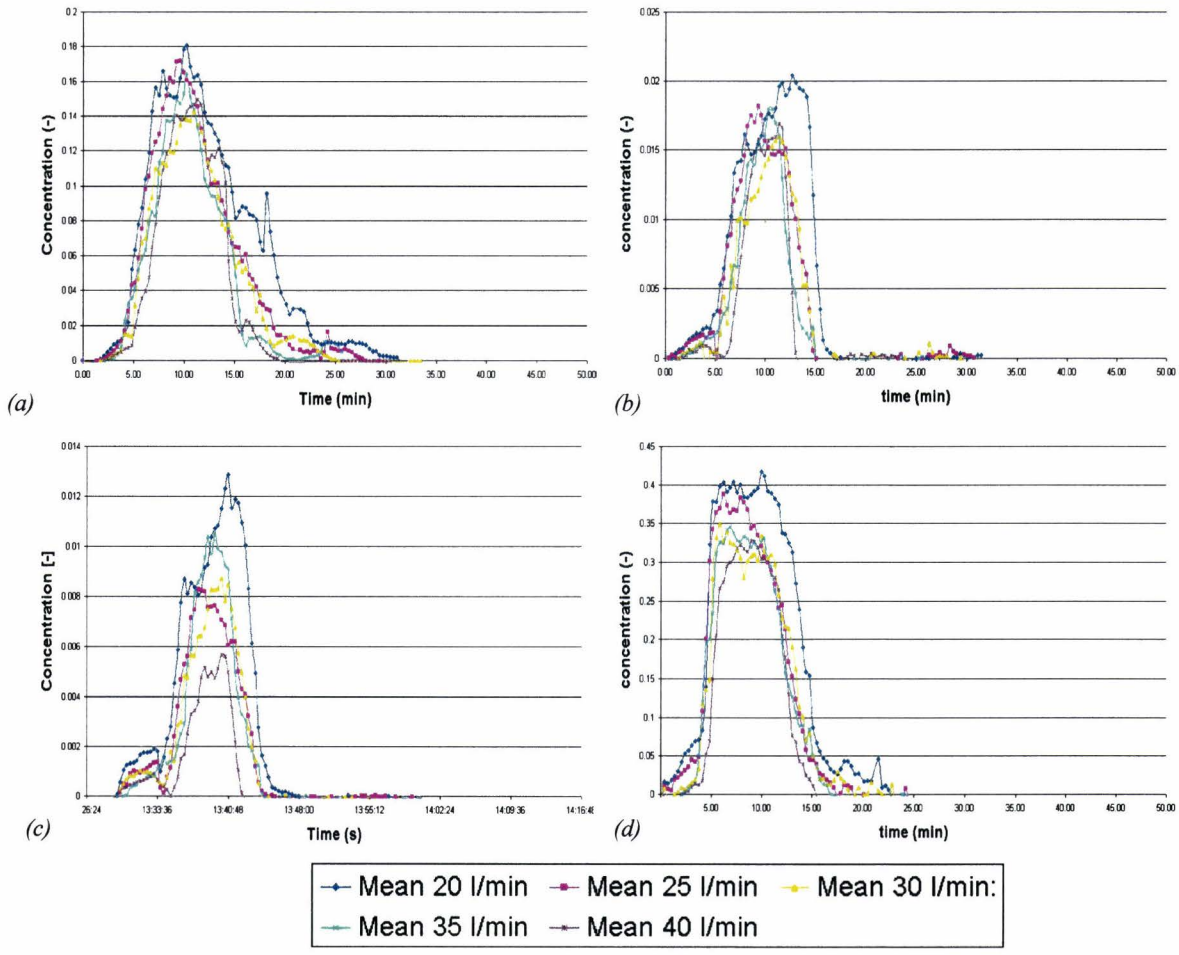

figure B-1: ***(a) Emission of CO, (b) emission of CH_4, (c) emission of NH_3, and (d) the emission of H_2O as function of the airflow at an oxygen concentration of 21%***

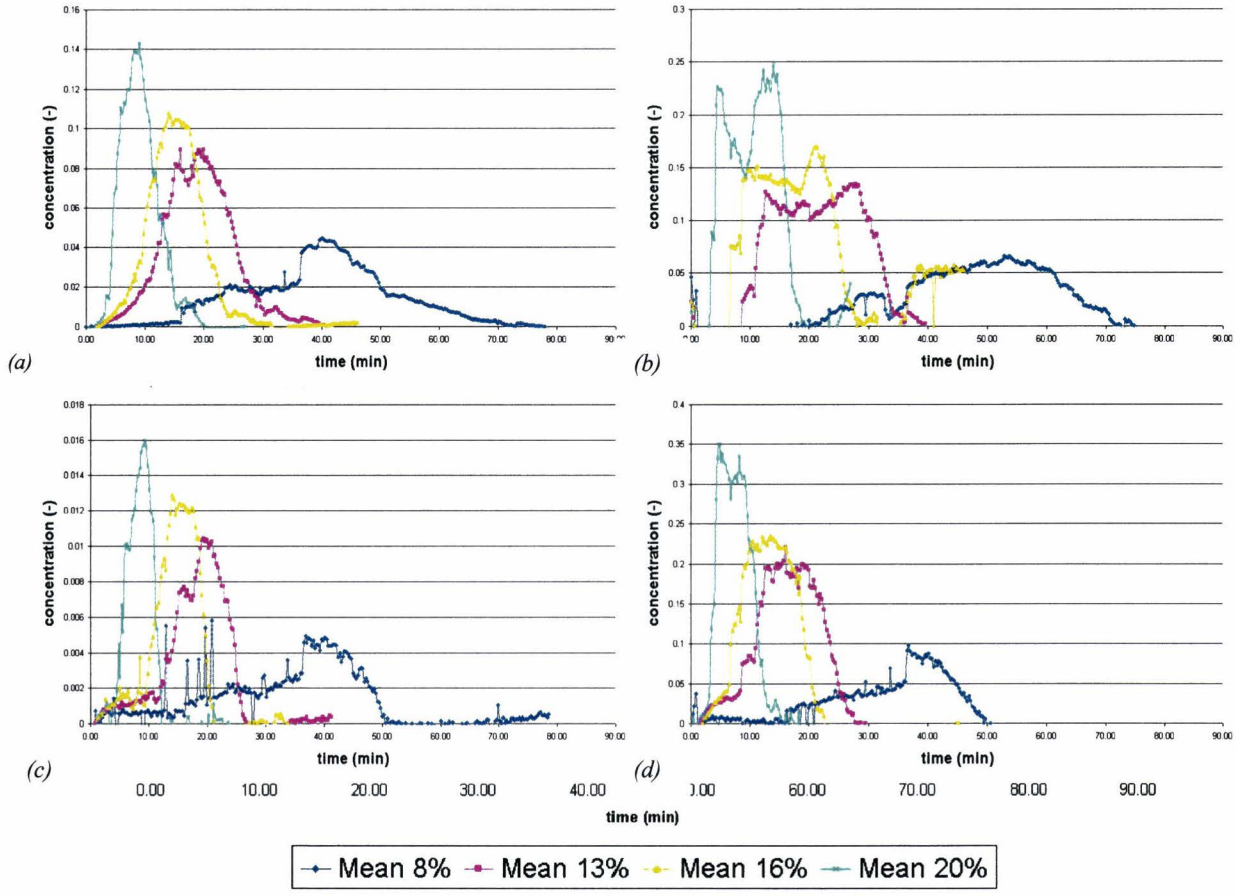

figure B-2: *(a) Emission of CO, (b) emission of CO_2, (c) emission of CH_4, and (d) emission of H_2O as function of the oxygen concentration at a mean airflow of 30 l/min.*